11-29-2017

A Geophysical Investigation of Stratigraphy and Structure on St. Catherines Island, Georgia

Anne M. DeLua
Georgia Southern University

A Geophysical Investigation of Stratigraphy and Structure on St. Catherines Island, Georgia

An Honors Thesis submitted in partial fulfillment of the requirements for Honors for the degree of Bachelors of Science in Geology.

By

Anne DeLua

Under the mentorship of Dr. R. K. Vance

ABSTRACT

Geophysical tools were used to investigate potential structural and stratigraphic pathways of the salt water intrusion that is affecting the surficial aquifer on St. Catherines Island, Georgia. Ground penetrating radar (GPR) is a geophysical tool that uses electromagnetic waves to view the subsurface. GPR is used for a variety of applications stratigraphically, biologically, and anthropogenically. GPR electromagnetic waves react to changes in density and composition and type and percentage of pore fluids in sediment and rock. GPR waves also react to interfaces including fractures and faults. GPR waves exhibit attenuation and decreased return signal in materials such as clay. Fresh water saturation of sand also attenuates GPR waves and saline waters may result in total loss of return signal. Therefore, it may be possible to use GPR to detect where salt water intrusion is occurring on the island and structural and stratigraphic pathways that permit it. Here we use a MALÅ ground-penetrating radar to determine where salt water is intruding into the shallow wells that have been dug on St. Catherines Island. We also use this data to create a more complete stratigraphical picture of the island. We found structural conduits in the shallow aquifer that may permit salt water intrusion. The ability to locate conduits is important because it allows for a greater understanding of salt water intrusion in the Georgia Coastal aquifers.

Thesis Mentor:_____

Dr. R. K. Vance

Honors Director:_____

Dr. Steven Engel

April 2017
Department of Geology and Geography
University Honors Program
Georgia Southern University

Table of Contents

Acknowledgements 3
INTRODUCTION 4
Research Site – St. Catherines Island 4
Previous Work 4
The Project 5
GEOPHYSICAL METHODS 6
GPR 6
Electrical Resistivity Tomography (ER) 7
GEOPHYSICAL INVESTIGATIONS ON SCI 8
GPR 8
GPR Data Processing 9
ER 9
RESULTS AND DISCUSSION 10
References Cited 11
Appendix 1: Figures 14
Appendix 2: Data 23

Acknowledgements

I would like to thank my advisor Dr. Vance as well as Dr. Kelly and Dr. Reichard for their contributions to this project.

Funding for this study was provided by the Georgia Sea Grant, St. Catherines Island Research Foundation, and Georgia Southern University.

INTRODUCTION

Research Site – St. Catherines Island

St. Catherines Island (SCI) is one of the barrier islands that lie along the Georgia coast and is situated near the center of the Georgia Bight. As seen in Figure 1, it is located about 35 miles south of Savannah, Georgia. It is managed by the St. Catherines Island foundation who have dedicated it for research, education and conservation. The island is made of approximately 22,000 acres of land with a variety of environments. These environments include salt marshes, barrier beaches, and an assortment of maritime forests (St. Catherines Island Foundation, 2015). As seen in Figure 2, the island has a Pleistocene core surrounded by a Holocene ridge and swale terrain and salt marsh (Vance et al., 2011). The Pleistocene core is covered by Holocene eolian sands that thin westward. On the western side of the core, which has been found to be topographically lower than the eastern side, there existed in the colonial period , fresh water springs and freshwater marshes that are now limited to ephemeral wetlands and ponds fed by pumping withdrawals from the Upper Floridan aquifer. The Floridan aquifer lies beneath five different states and is one of the most productive aquifers in the world (Figure 3).

Previous Work

It is believed that the locality of former artesian springs on St. Catherines Island (SCI) was mainly fault and joint controlled and those structures and pathways may now be one of the conduits that allow saltwater intrusion into the Upper Floridan aquifer of the island (Reichard et al., 2014). In a study by Vance et al. (2011), sag structures were found on St. Catherines that may have formed by cavern collapse in the Upper Floridan aquifer.

The solution activity that created the sag structures was focused along the joints and faults that are now conduits for saltwater intrusion in the Upper Floridan. Subsequent studies by Reichard and co-workers have identified chloride spikes in the surficial aquifer indicating it is also experiencing salt water intrusion. To investigate salt water intrusion in the surficial aquifer, thirteen additional shallow wells (<24 ft.) were drilled in 2016 to complete an eighteen well grid system. Additional sampling verifies salt water intrusion in the shallow aquifer; however, the occurrence in specific wells is not consistent with simple lateral intrusion along permeable strata (Reichard, Vance, Kelly, pers. Communication, 2016).

The Project

My research focus was on understanding the shallow surficial aquifer and finding where it is becoming contaminated with salt water. There are conduits passing through both the shallow and deep aquifers that allow for salt water contamination in the Upper Floridan aquifer and permitted Artesian spring flow in the past. Reichard et al. (2014) concluded in their study that these conduits are near-vertical joints, faults, and/or solution collapse features. Those same conduits may be responsible for lateral or vertical intrusion of salt water into the surficial aquifer (Vance, pers. communication, 2017).

I believe Ground Penetrating Radar (GPR) and Electrical Resistivity (ER) may be used to locate zones of enhanced permeability and structural features (faults, joints) in the shallow surficial strata that are conduits for the saltwater intrusion. By combining GPR and ER with core data I can create a more complete picture of the stratigraphy and structure of the island. This project is significant because it will allow for a more precise

understanding of salt water intrusion mechanisms along the Georgia coast and barrier islands in general, as well as potentially affecting policy on groundwater management.

GEOPHYSICAL METHODS

GPR

Ground penetrating radar (GPR) is a non-invasive system that is often used to detect underground structures, soil, and rock formation by using electromagnetic radiation, seen in Figure 4. This system is very useful for detecting changes in soil and sediment type and differences in hydrology (Peterson et al., 2007), as well as buried objects (Pasolli et al., 2009). Baker et al (2007) describe a variety of terms and formulas needed to completely understand the complexities of the radar. This includes many of Maxwell's equations, such as, $v_p = \frac{1}{\sqrt{\mu_0 \mu_r \varepsilon_0 \varepsilon_r}}$, which describes the phase velocity and therefore, propagation of an electromagnetic wave through a material. Maxwell's equations in general describe the relationship between electromagnetic properties and wave propagation. It is important to have a grasp of the terms as they relate to geology because they are often used in other disciplines in a slightly different way. GPR is a very useful tool when examining structures under the surface, but has a variety of limitations that should be kept in mind when setting up a study area. Different types of sediments affect the signals from GPR (Bristow and Jol, 2003; Baker et al., 2007), especially clays. Clays, and other materials that do not transmit waves well, cause attenuation. This is the extinction of the wave as it travels underground and leads to unusable data (Bristow and Jol, 2003; Baker et al., 2007; Hatch et al., 2013; Schmelzbach and Huber, 2015). There are a few methods that have been created to decrease attenuation or allow the data to be

understandable, such as efficient deconvolution (Schmelzbach and Huber, 2015). Attenuation is a rather large limitation of the system, although it can be used to detect salt water and clays (Bristow and Jol, 2003; Hatch et al., 2013). With this in mind, proper location, soil types, and antenna orientation are critical for obtaining the best results possible in the given area (Bristow and Jol, 2003; Baker et al., 2007; Doetsch et al., 2012). GPR can also be combined with other systems, such as electrical resistivity tomography, to produce more accurate results (Doetsch et al., 2012).A number of studies have used GPR to analyze beach ridges and barrier islands (Thomas et al., 1978; Johnston et al., 2007; Peterson et al., 2007; Vance et al., 2011). Johnston et al. (2007) created a conceptual model to explain beach ridge formation using GPR and vibracore data that can be easily related to formations on barrier islands, such as St. Catherines Island. Peterson et al. (2007) studied groundwater and its contamination using GPR, which pertains to the salt water intrusion of aquifers on the East Coast. GPR studies of St. Catherines Island have been done before; for example, Vance et al. (2011) investigated the stratigraphy and structure of the island, and hydrologic implications (Figure 5).

Electrical Resistivity Tomography (ER)

Electrical resistivity (ER) is another non-invasive system used to detect subsurface features using an electrical current. The current is sent through the subsurface, reflecting back to the electrical nodes with different angles based on the resistances of the different materials in the subsurface (Van Dam, 2010; Loke et al., 2013). ER is a very useful tool when studying coastal aquifers due to the large difference in resistivity between freshwater and saltwater, with the former having a higher resistivity and the latter having a lower resistivity (Dimova et al., 2012). Combing ER with GPR is very useful because

conductivity, which GPR measures, is inversely related to resistivity, showing a more complete and clear picture of the subsurface.

GEOPHYSICAL INVESTIGATIONS ON SCI

As seen in Figure 6, a series of three well transects have been drilled across the island (Vance, personal communication 2016). Geophysical data was collected both perpendicular and parallel to these well transects, especially along the southern and middle transects. We had a total of 4 ER transects (Figure 7) and 18 GPR transects near well S4, along Savannah road, near Junction 80, and along State road and Back Creek road as seen in Figure 8. GPR data was gathered in November of 2016 and January of 2017, with ER data gathered in the November trip. Water sampling was done on both trips as well.

GPR

A MALÅ ground-penetrating radar system consisting of a Ramac X3M controller and monitor paired with either 100 MHz or 250 MHz shielded antennae as shown in Figure 9. The antennae incorporate both a transmitter and receiver in one unit. The controller-antenna system was used in sled mode for both the 100 and the 250 MHz antennae, towing the sled behind a John Deere Gator ATV. The MALÅ Ramac monitor (Figure 10) was used to calibrate and configure the system and record data and profile markers. The compact, durable construction and simple operation made the monitor preferable to a laptop for prolonged field use. The system is powered by a lithium-ion battery that provides ~5 hours of use. A second, fully charged backup battery ensured a full day of use. Survey data recorded in the monitor was saved to a laptop for processing with

MALÅ software. Profiles were treated by identification of radar surfaces and by grouping radar reflection elements into packages or associations and radar facies. The ground radar waves reacted to changes in subsurface physical properties that may or may not coincide with bedding surfaces or structures.

GPR Data Processing

The MALA software used for data acquisition and processing include GroundVision and Object Mapper. The velocity of the radar waves used for depth modelling was calculated from diffraction hyperbolae obtained previously from Vance et al., (2011) using the MALA Radar Explorer program and checked against the ground truth provided by core data. Filtering of raw GPR data included DC (direct current) adjustment, FIR, time gain and average, and delete mean trace. The ground velocity was set at 65 m/μs for the 250 MHz profiles and 55 m/μs for the 100 MHz profiles.

ER

We used the Super Sting R8/IP Marine Electrical Resistivity Meter by Advanced Geosciences Inc. as shown in Figure 11. The cable itself is approximately 168 meters long with 56 take-outs spread across three meter intervals. We deployed the cable both parallel and perpendicular to the well transects and along the sag structure near well S4, fixing it to the ground with metal stakes as seen in Figure 12. Due to the relative resistivity of the surface, saltwater was poured around the stakes to allow for better ER readings. A dipole-dipole configuration was used, allowing for data collection of up to 40 meters in depth. Before every data collection, a series of tests were run to insure the proper working order of the cable including a receiver test, a relay test, and a cable test.

Once data was collected, Earth Imager 2D by Advanced Geosciences Inc. was used to process the images. The inversion was used to define a model that predicts the true resistivity values under the electrode configuration used when collecting the data.

RESULTS AND DISCUSSION

Preliminary results have shown multitudes of small fractures (Figure 13) that could potentially be linked to deeper faults in the Floridan aquifer. In soft sediments, such as clay and sand, the deeper faults propagate and splay out into smaller fractures as they move towards the surface. Figure 14 shows multiple fractures, highlighted in red, and a band of attenuation that could be a change in layer type from a sand to a clay or possibly the beginning of the water table. The faults and joints found in these profiles could potentially permit the former artesian springs to flow and are now the modes allowing for the salt water intrusion. We also located several sag structures which we believe to have been formed by the collapse of the Floridan aquifer (Figures 15 and 16). These structures could be linked to the irregularities of the salt water intrusions amongst the wells. The sag structures can also be seen in the electrical resistivity profiles of the area (Figure 17). The ability to see the sag structures strongly correlated in both GPR and ER profiles indicates the usefulness of using these geophysical methods together. There are still other potential modes of salt water intrusion to be discovered in future research using these methods such as buried paleochannels.

References Cited

Baker, G.S., Jordan, T.E., and Pardy, J., 2007, An introduction to ground-penetrating radar (GPR): Special Paper - Geological Society of America, v. 432, p. 1-18.

Bristow, C.S., and Jol, H.M., 2003, An introduction to ground penetrating radar (GPR) in sediments: Geological Society Special Publications, v. 211, p. 1-7.

Dimova, N.T., Swarzenski, P.W., Dulaiova, H., and Glenn, C.R., 2012, Utilizing multichannel electrical resistivity methods to examine the dynamics of the freshwater-seawater interface in two Hawaiian groundwater systems: Journal of Geophysical Research, v.117, p. 1-12.

Doetsch, J., Linde, N., Pessognelli, M., Green, A.G., and Guenther, T., 2012, Constraining 3-D electrical resistance tomography with GPR reflection data for improved aquifer characterization: Journal of Applied Geophysics, v. 78, p. 68-76.

Hatch, M.A., Heinson, G., Munday, T., Thiel, S., Lawrie, K., Clarke, J.D.A., and Mill, P., 2013, The importance of including conductivity and dielectric permittivity information when processing low-frequency GPR and high-frequency EMI data sets: Journal of Applied Geophysics, v. 96, p. 77-86.

Johnston, J.W., Thompson, T.A., and Baedke, S.J., 2007, Systematic pattern of beach-ridge development and preservation; conceptual model and evidence from ground-penetrating radar: Special Paper - Geological Society of America, v. 432, p. 47-58.

Loke, M.H., Chambers, J.E., Rucker, D.F., Kuras, O., Wilkinson, P.B., 2013, Recent developments in the direct-current geoelectrical imaging method: Journal of Applied Geophysics, v. 95, p. 135-156.

Pasolli, E., Melgani, F., and Donelli, M., 2009, Automatic Analysis of GPR Images: A Pattern-Recognition Approach: IEEE Transactions on Geoscience and Remote Sensing, v. 47, no. 7.

Peterson, C.D., Jol, H.M., Percy, D., and Nielsen, E.L., 2007, Groundwater surface trends from ground-penetrating radar (GPR) profiles taken across late Holocene barriers and beach plains of the Columbia River littoral system, Pacific Northwest coast, USA: Special Paper - Geological Society of America, v. 432, p. 59-76.

Schmelzbach, C., and Huber, E., 2015, Efficient deconvolution of ground-penetrating radar data: IEEE Transactions on Geoscience and Remote Sensing, no. 9, p. 5209.

St. Catherines Island Foundation, St. Catherines Island, 2015: http://www.stcatherinesisland.org/.

Thomas, D.H., Jones, G.D., Durham, R.S., Larsen, C.S., and Moore, C.B., 1978, The anthropology of St. Catherines Island. 1, Natural and cultural history.: Anthropological Papers of the American Museum of Natural History, v. 55, no. 2.

Van Dam, R.L., 2010, Landform characterization using geophysics- Recent advances, applications, and emerging tools: Geomorphology, p. 57-73.

Vance, R.K., Trupe, C.H., and Rich, F.J., 2009, Integrating ground-penetrating radar and traditional stratigraphic study in an undergraduate field methods course: Special Paper - Geological Society of America, v. 461, p. 155-161.

Vance, R.K., Bishop, G.A., Rich, F.J., Meyer, B.K., and Camann, E.J., 2011, Application of ground penetrating radar to investigations of the stratigraphy, structure, and hydrology of St. Catherines Island: Anthropological Papers of the American Museum of Natural History, v. 94, p. 209-236.

Appendix 1: Figures

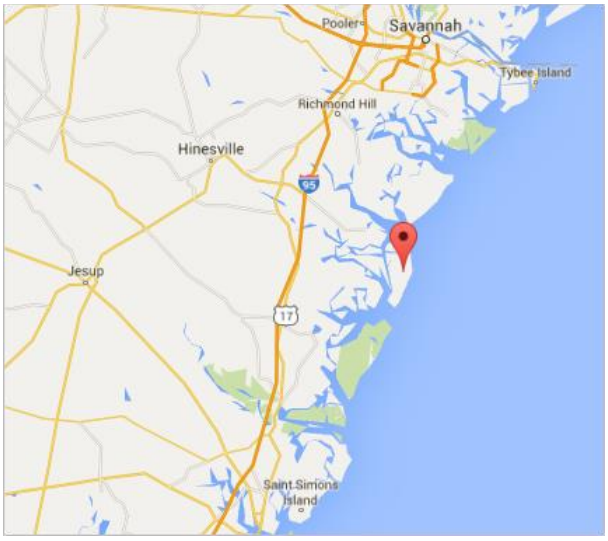

Figure 1: Map of Southeast Georgia and its barrier islands. The red marker is located on St. Catherines Island. Image taken form Google Earth.

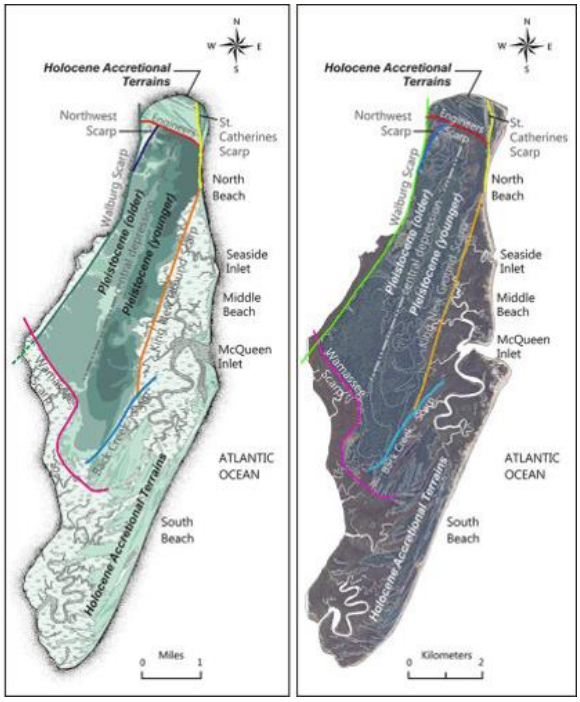

Figure 2: Map showing the outline of the Pleistocene core and outer Holocene terrain on St. Catherines Island. Image taken from http://www.stcatherinesisland.org/.

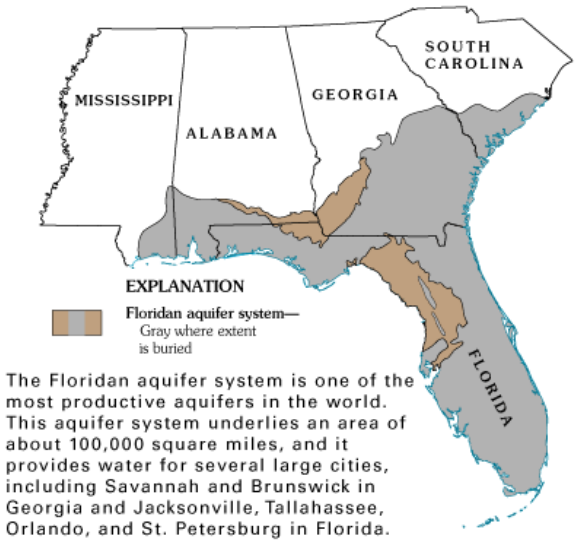

Figure 3: Image showing the outlines of the Floridan Aquifer System, taken from USGS.

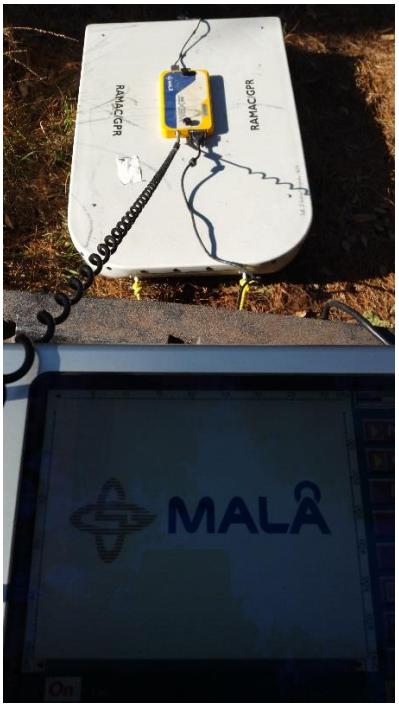

Figure 4: GPR set-up using 100 MHz antenna being dragged behind a John Deer Gator. Personal Image.

Figure 5: Dr. Vance operating the GPR system on St. Catherines Island. Image courtesy of Dr. Vance.

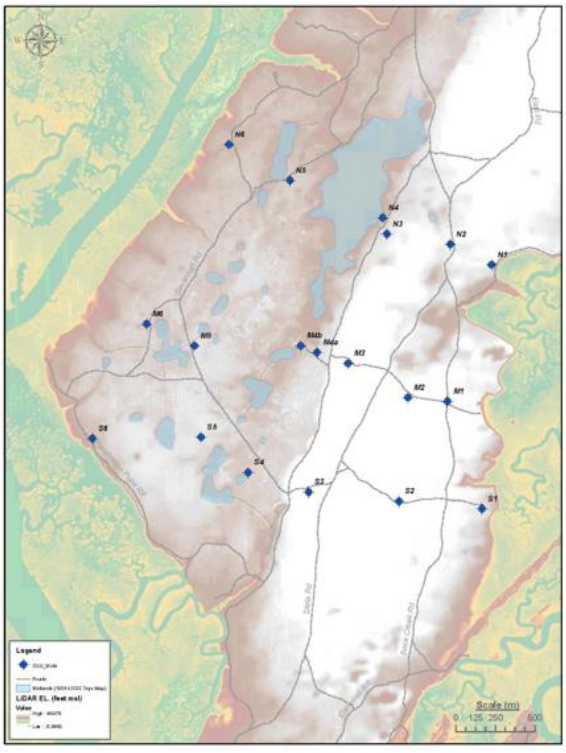

Figure 6: Zoom in of St. Catherines Island showing location of three well transects. Blue diamonds represent well sites. Image courtesy of Dr. Vance.

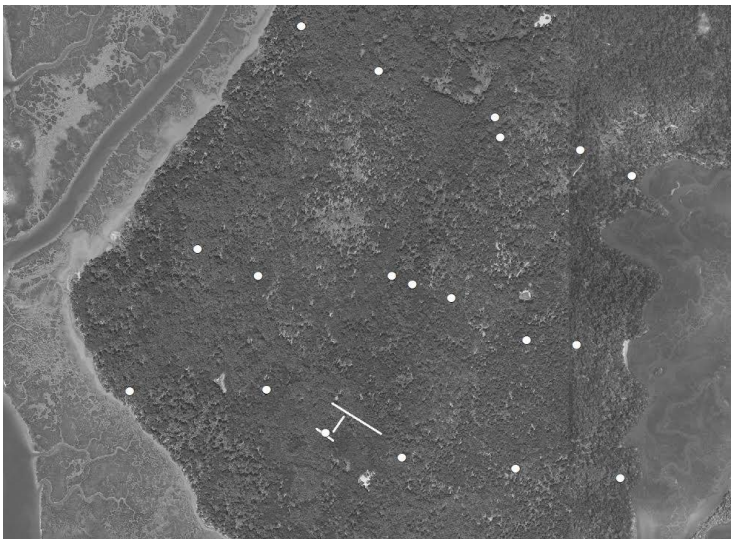

Figure 7: Image of St. Catherines Island where white dots represent well sites and white lines represent ER transects. Image courtesy of Dr. Kelly.

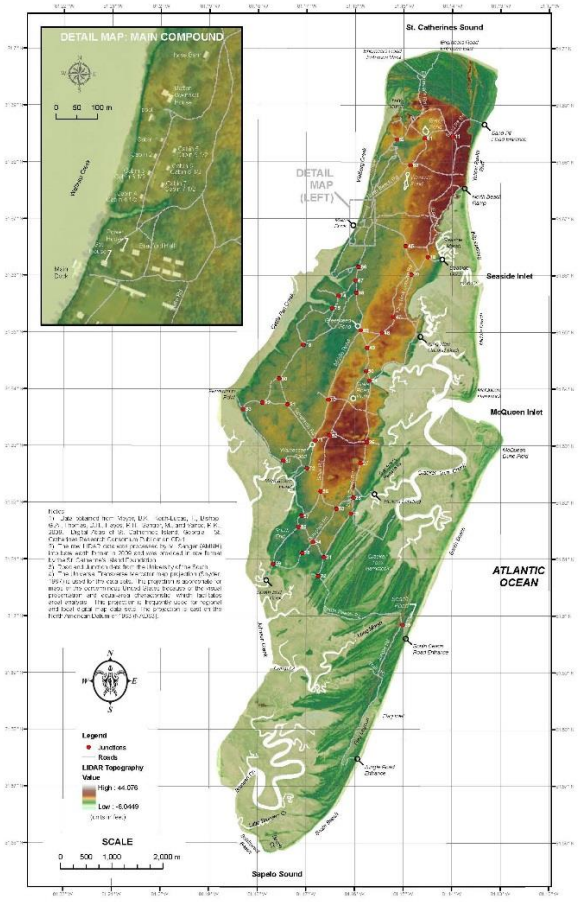

Figure 8: Image of St. Catherines Island with red dots indicating road junctions. Image courtesy of Dr. Vance.

Figure 9: 250 MHz antenna being used on St. Catherines Island along State Road. Personal Image.

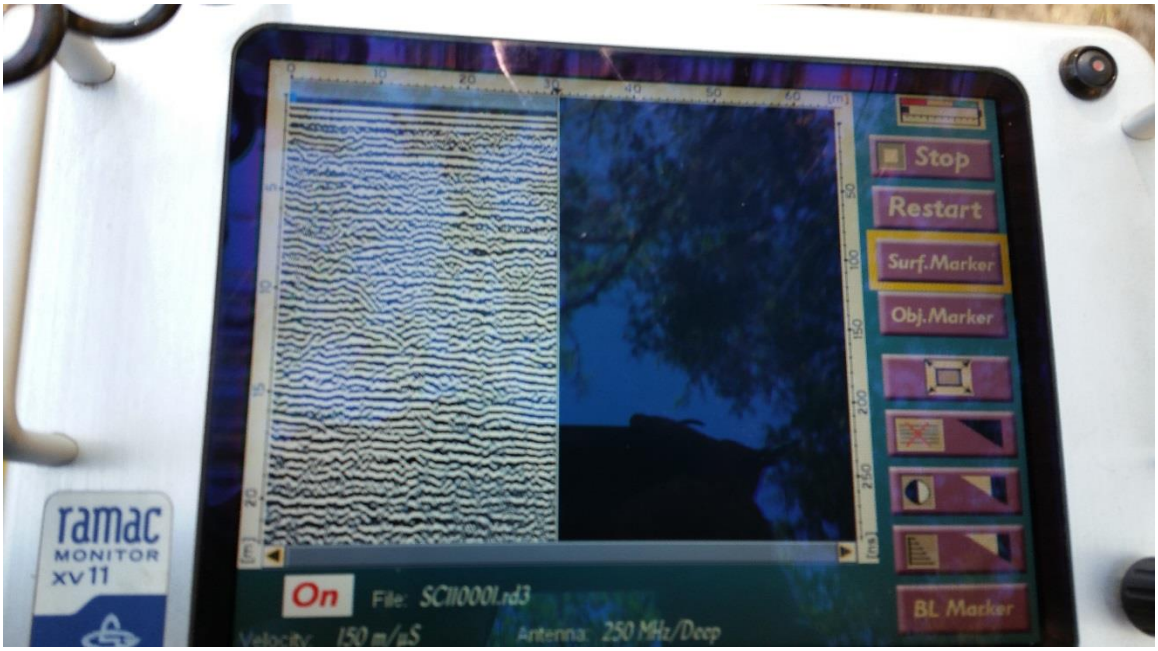

Figure 10: Image showing the Ramac monitor screen while GPR is running. Personal Image.

Figure 11: Image of the Supersting Marine control systems. Personal image.

Figure 12: Electrical resistivity node that has been staked to the ground and surrounded by saltwater on St. Catherines Island. Personal image.

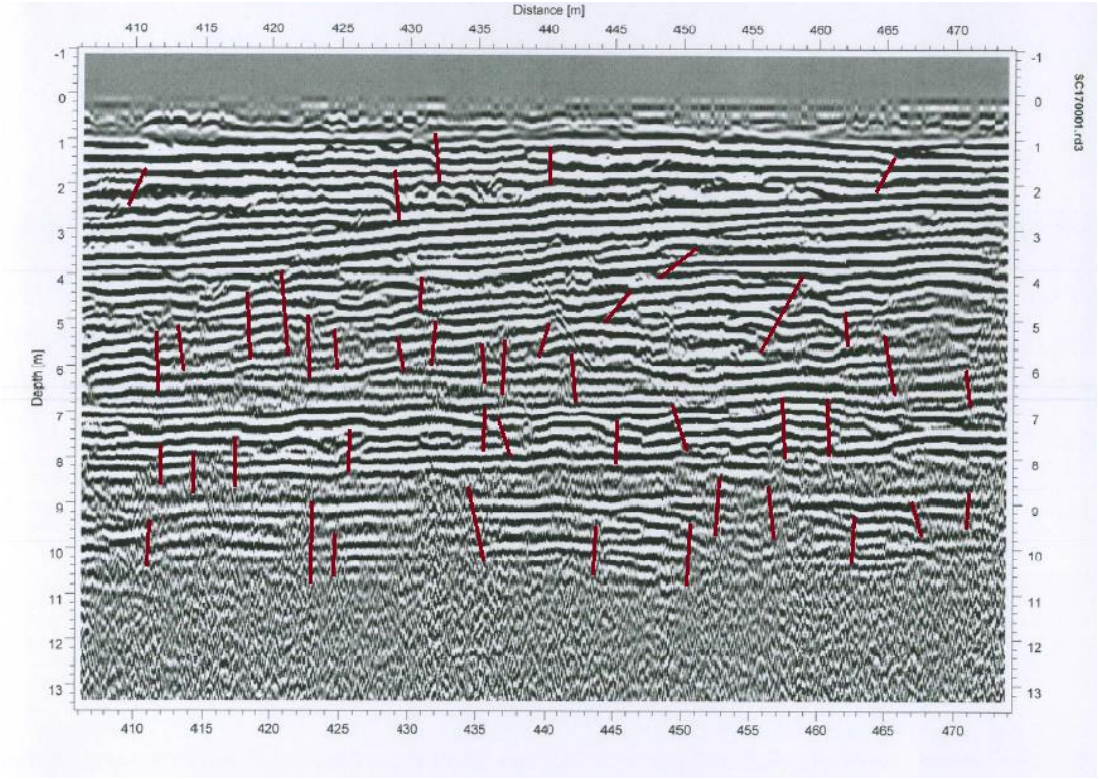

Figure 13: Image 7 of GPR Profile 4 that highlights fracturing in the subsurface.

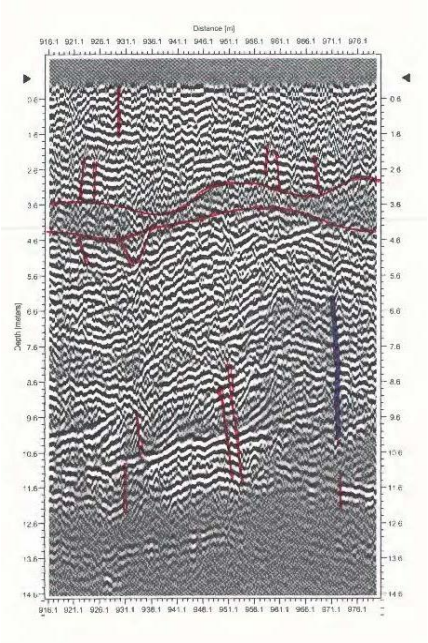

Figure 14: Image 7 of GPR Profile 1 that highlights various fracturing and a highly attenuated layer.

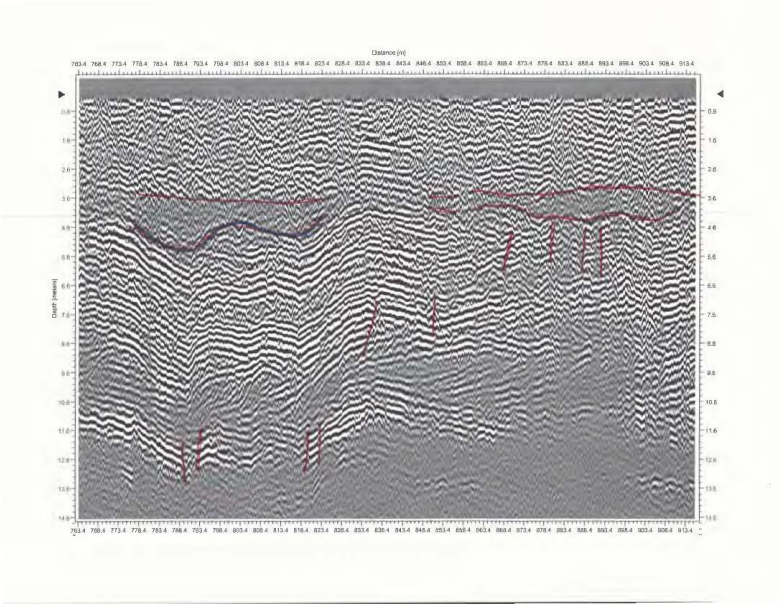

Figure 15: Image 6 of GPR Profile 1 shows the top of the sag structure highlighted in blue. Directly above that, highlighted in red, shows the attenuated layer seen in the previous image.

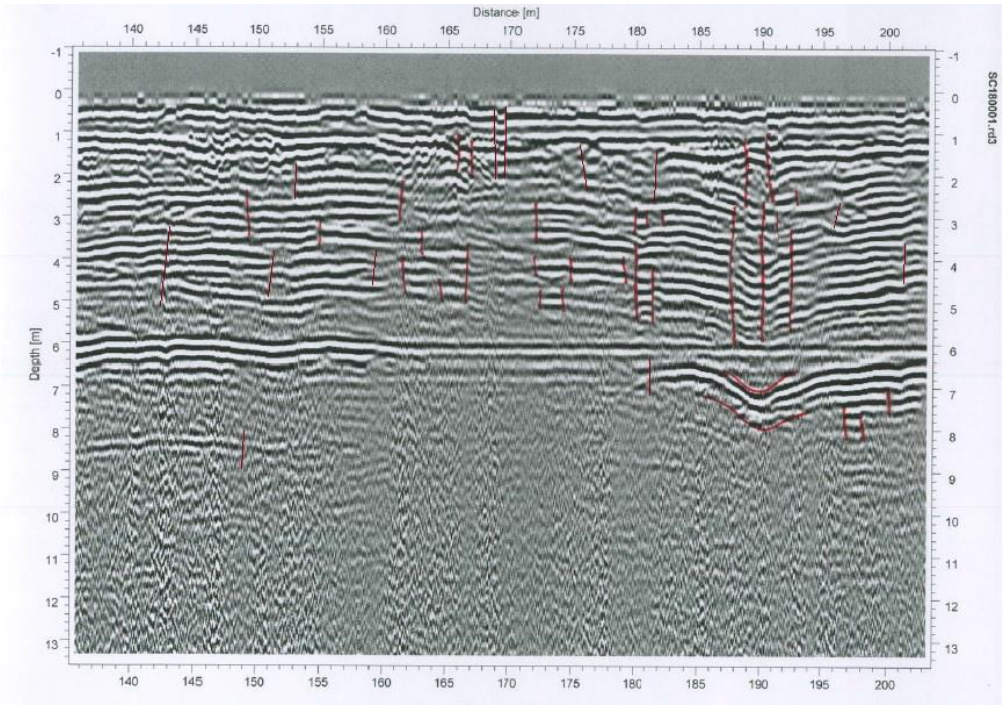

Figure 16: Image 3 of GPR Profile 5 showing a sag structure in the right hand side along with a multitude of fractures.

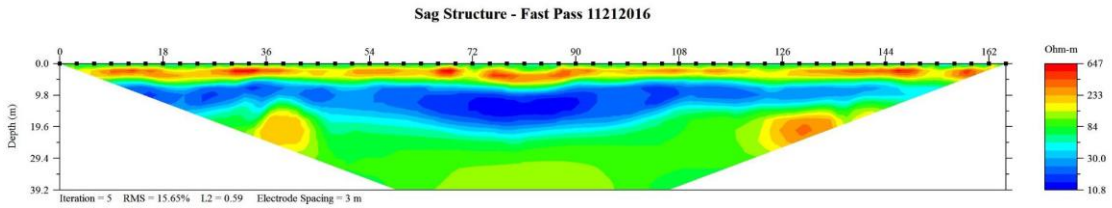

Figure 17: Electrical resistivity data showing a sag structure from approximately 72 to 90 meters in distance. The sag can be seen most directly in the yellow layer which indicates a high level of resistivity.

Appendix 2: Data

GPR Profiles

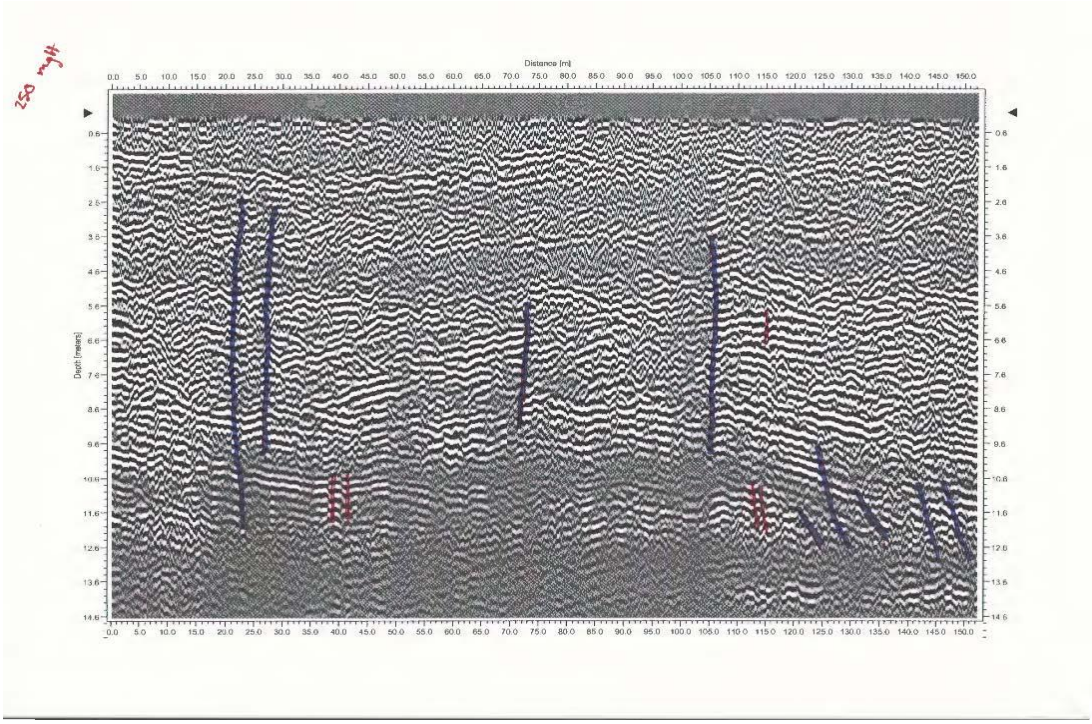

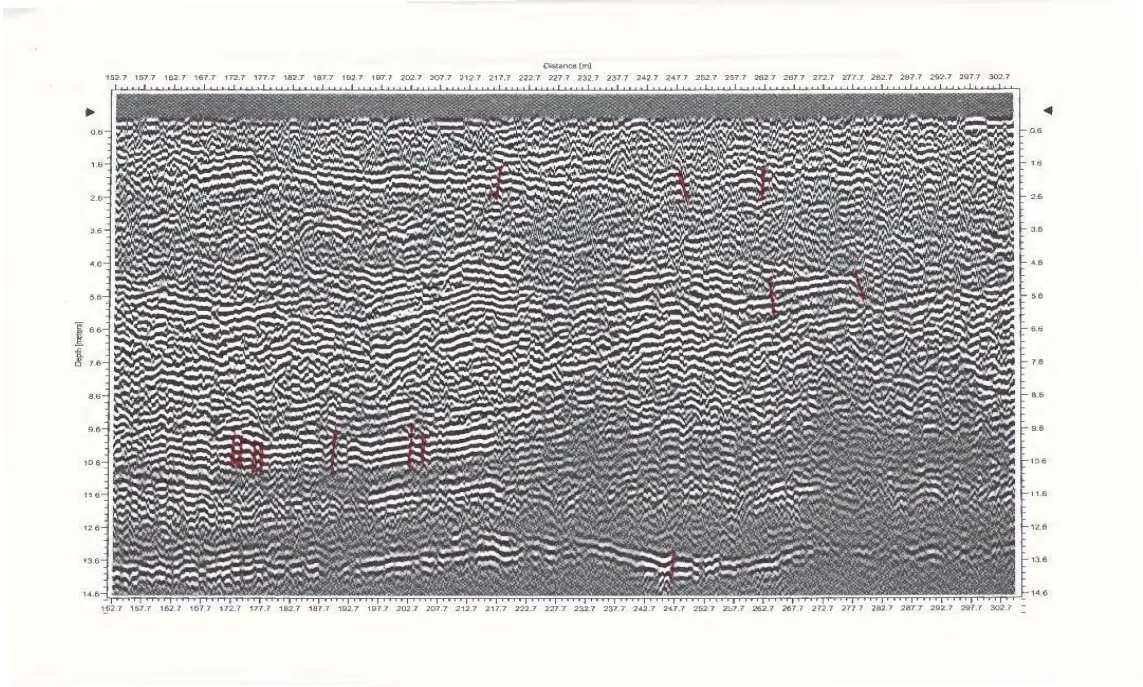

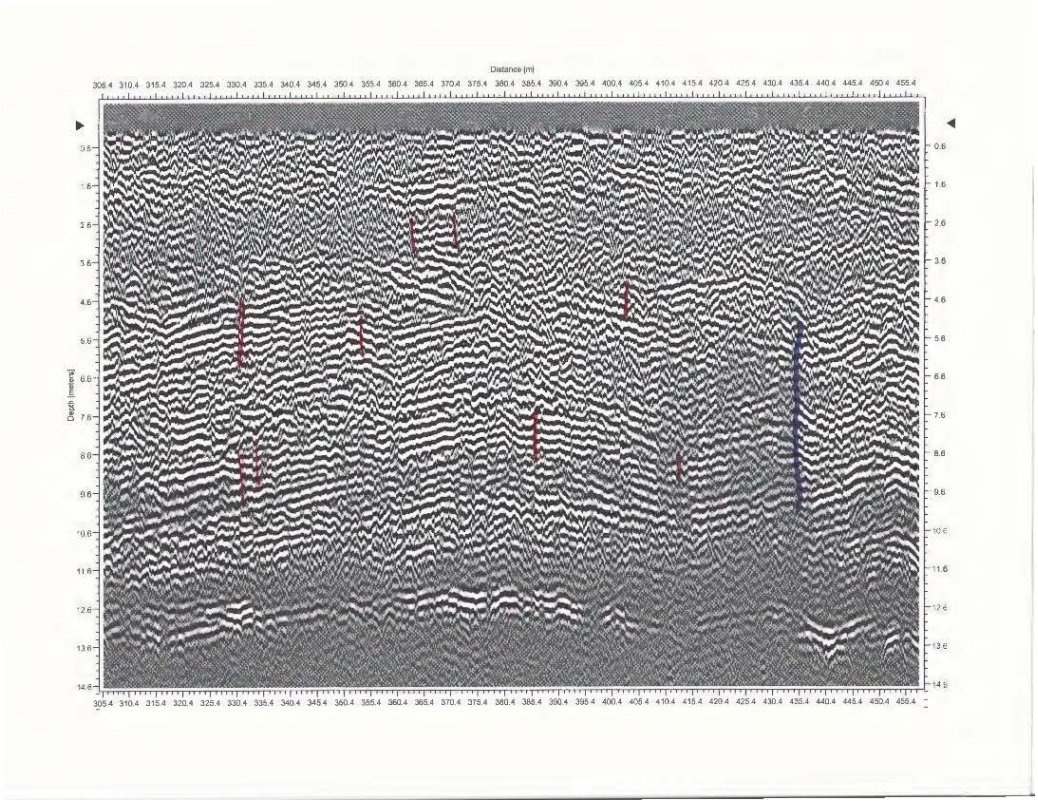
Distance [m]
Depth [meters]

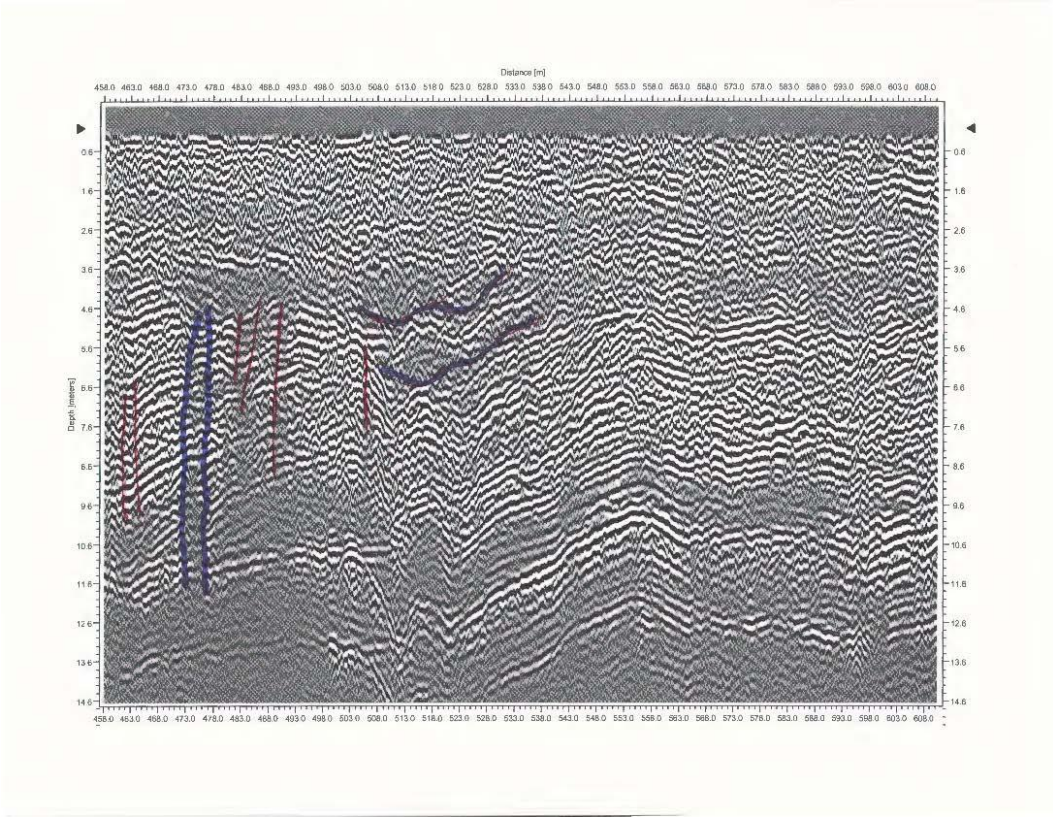
Distance [m]
Depth [meters]

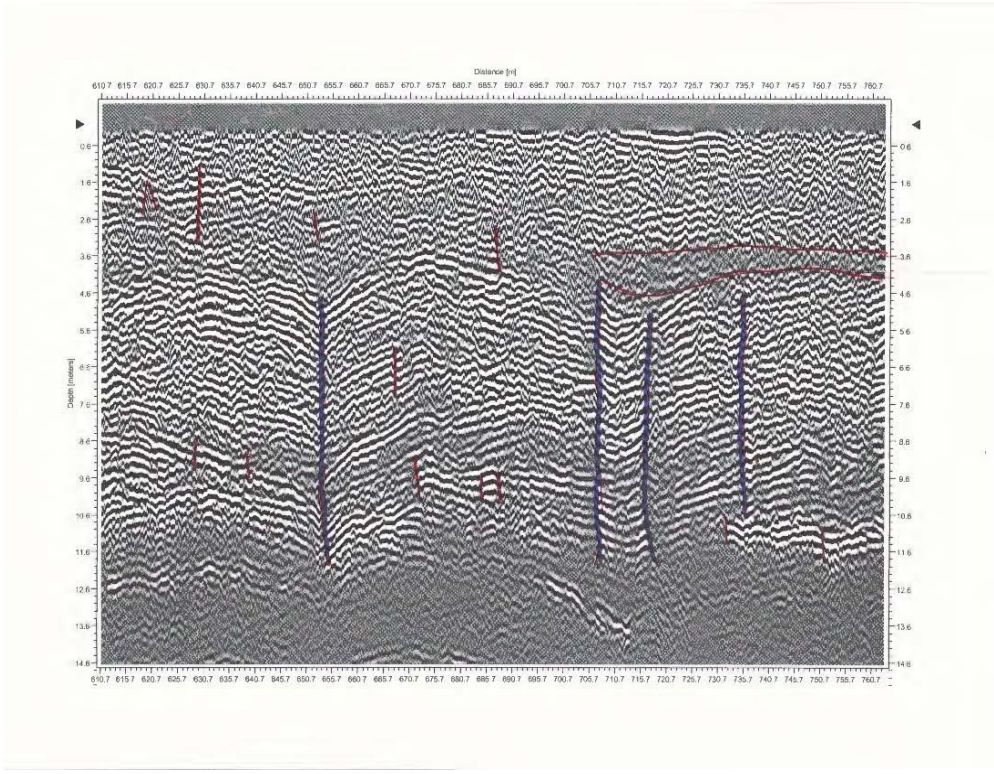
Distance [m]
610.7 615.7 620.7 625.7 630.7 635.7 640.7 645.7 650.7 655.7 660.7 665.7 670.7 675.7 680.7 685.7 690.7 695.7 700.7 705.7 710.7 715.7 720.7 725.7 730.7 735.7 740.7 745.7 750.7 755.7 760.7
Depth [meters]

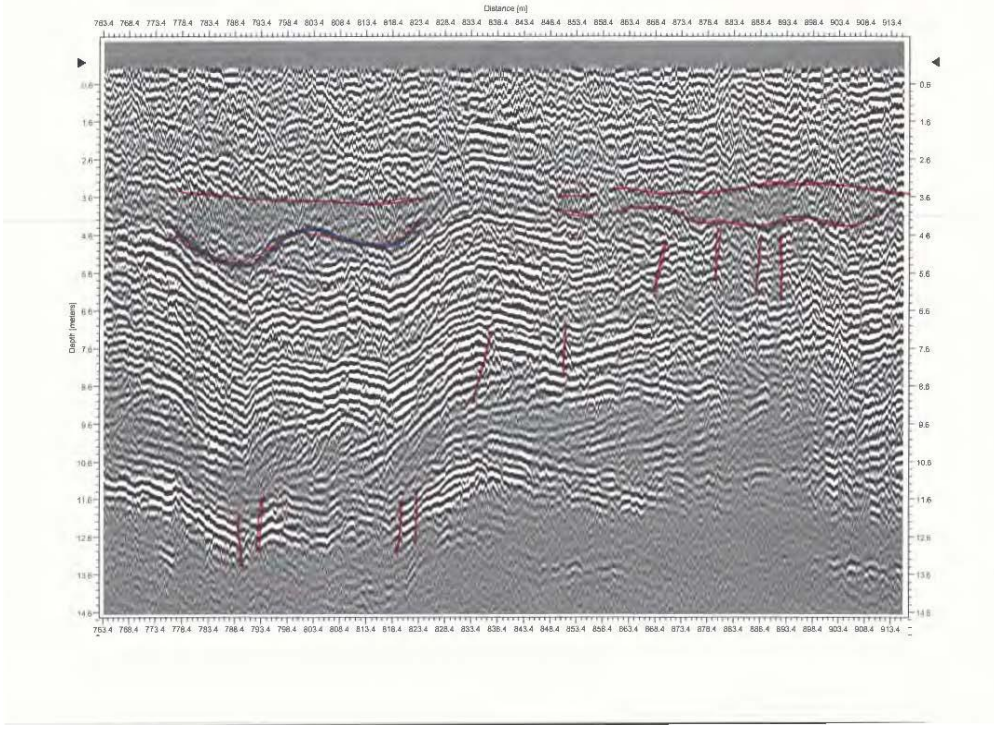
Distance [m]
763.4 768.4 773.4 778.4 783.4 788.4 793.4 798.4 803.4 808.4 813.4 818.4 823.4 828.4 833.4 838.4 843.4 848.4 853.4 858.4 863.4 868.4 873.4 878.4 883.4 888.4 893.4 898.4 903.4 908.4 913.4
Depth [meters]

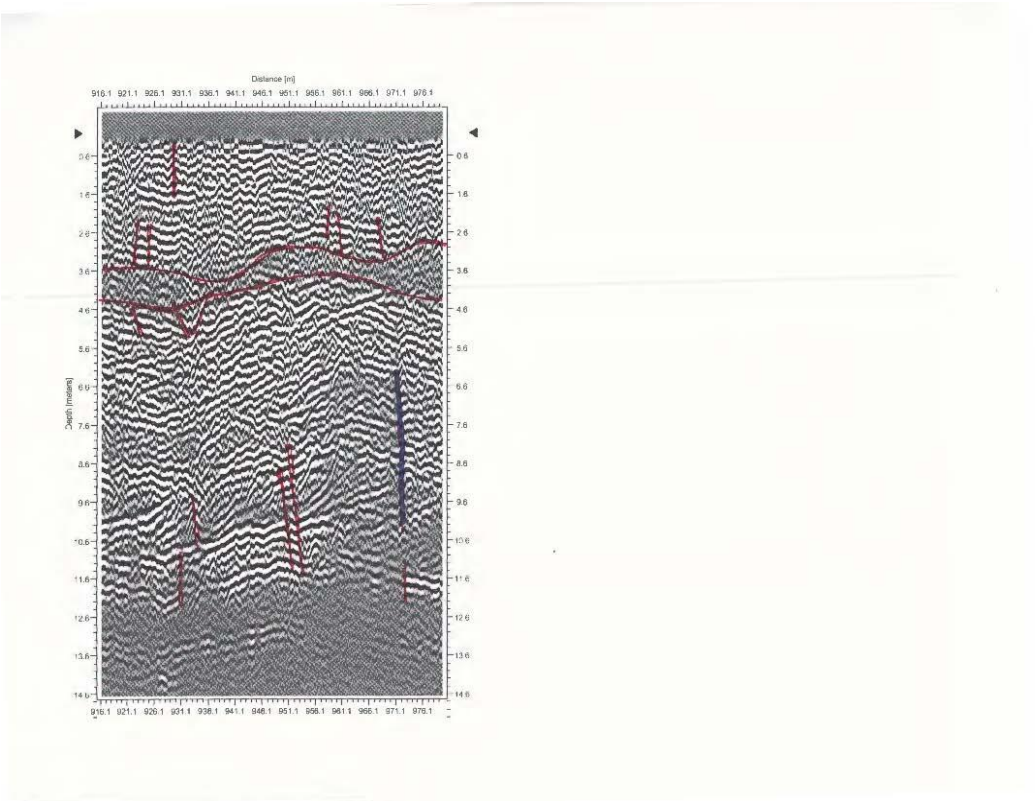

Profile 1 was run with the 250 MHz antenna from Junction 52 going north along State Road. The profile has a distance of 900 meters with a depth of 14.6 meters. Various faults, sag structures, and layer interfaces are highlighted in red. Excerpts of this profile are used in the results section.

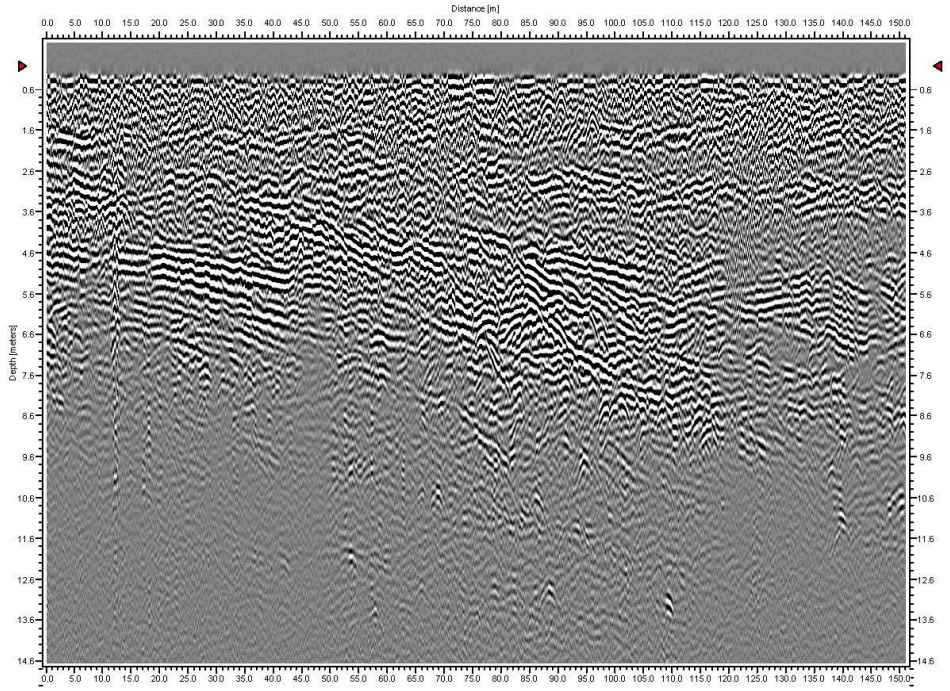
Distance [m]
0.0 5.0 10.0 15.0 20.0 25.0 30.0 35.0 40.0 45.0 50.0 55.0 60.0 65.0 70.0 75.0 80.0 85.0 90.0 95.0 100.0 105.0 110.0 115.0 120.0 125.0 130.0 135.0 140.0 145.0 150.0
Depth [meters]
0.6 1.6 2.6 3.6 4.6 5.6 6.6 7.6 8.6 9.6 10.6 11.6 12.6 13.6 14.6

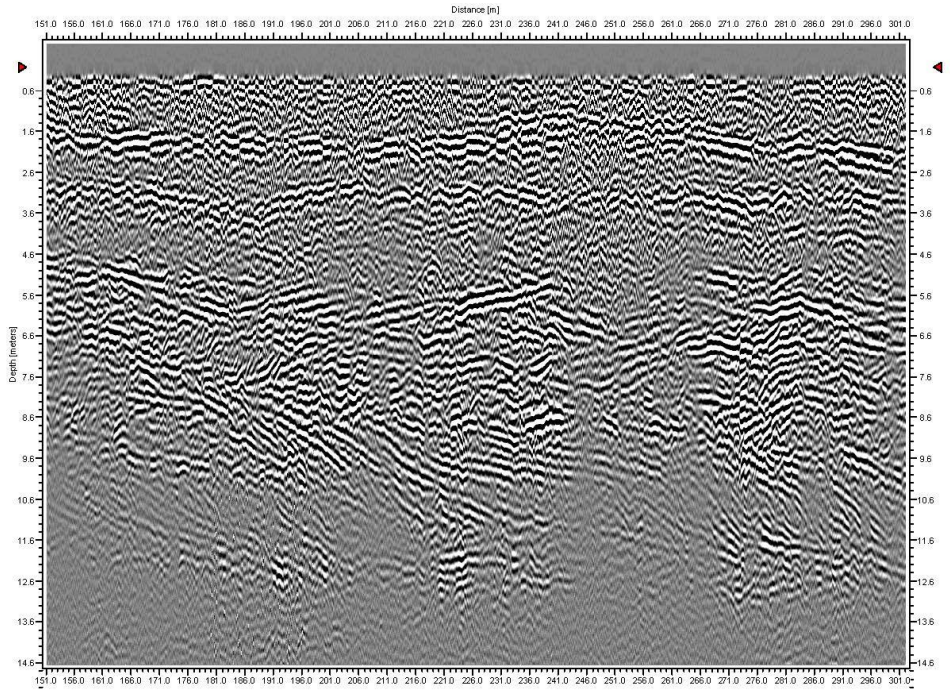
Distance [m]
151.0 156.0 161.0 166.0 171.0 176.0 181.0 186.0 191.0 196.0 201.0 206.0 211.0 216.0 221.0 226.0 231.0 236.0 241.0 246.0 251.0 256.0 261.0 266.0 271.0 276.0 281.0 286.0 291.0 296.0 301.0
Depth [meters]
0.6 1.6 2.6 3.6 4.6 5.6 6.6 7.6 8.6 9.6 10.6 11.6 12.6 13.6 14.6

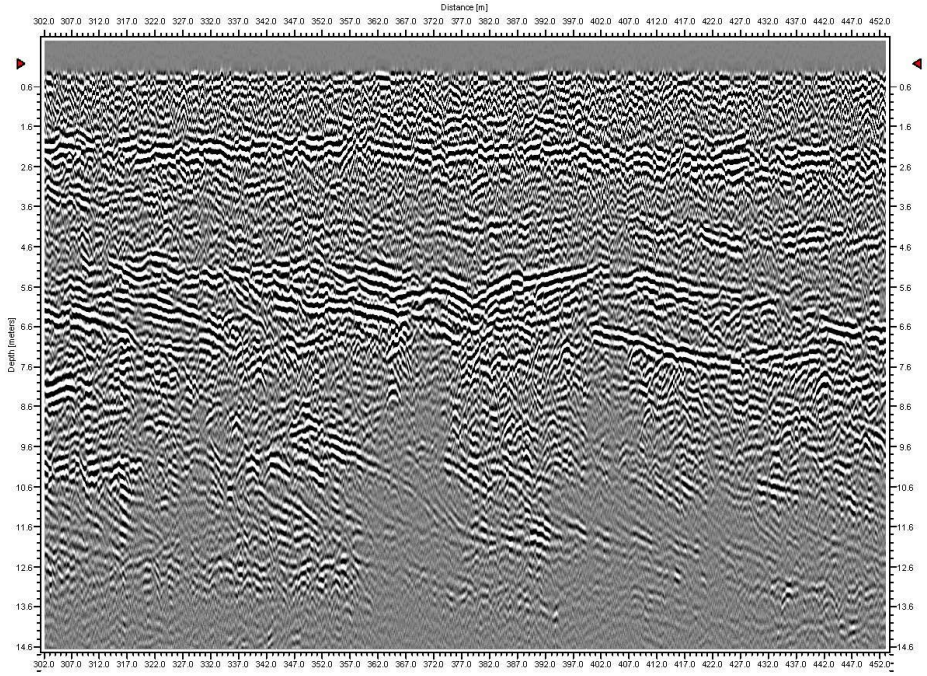
Distance [m]
302.0 307.0 312.0 317.0 322.0 327.0 332.0 337.0 342.0 347.0 352.0 357.0 362.0 367.0 372.0 377.0 382.0 387.0 392.0 397.0 402.0 407.0 412.0 417.0 422.0 427.0 432.0 437.0 442.0 447.0 452.0
Depth [meters]
0.6 1.6 2.6 3.6 4.6 5.6 6.6 7.6 8.6 9.6 10.6 11.6 12.6 13.6 14.6

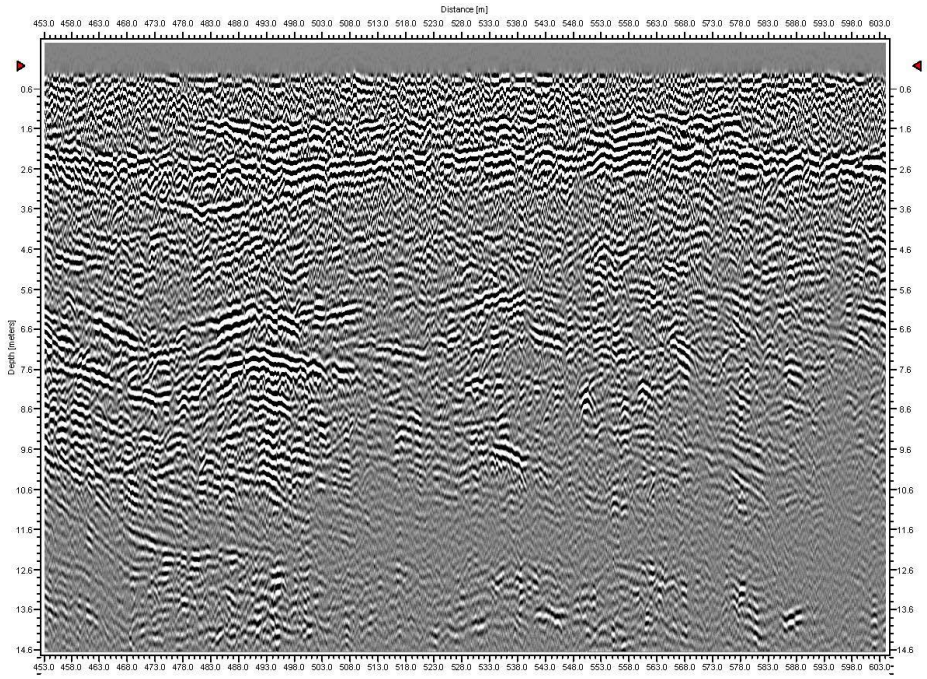
Distance [m]
453.0 458.0 463.0 468.0 473.0 478.0 483.0 488.0 493.0 498.0 503.0 508.0 513.0 518.0 523.0 528.0 533.0 538.0 543.0 548.0 553.0 558.0 563.0 568.0 573.0 578.0 583.0 588.0 593.0 598.0 603.0
Depth [meters]
0.6 1.6 2.6 3.6 4.6 5.6 6.6 7.6 8.6 9.6 10.6 11.6 12.6 13.6 14.6

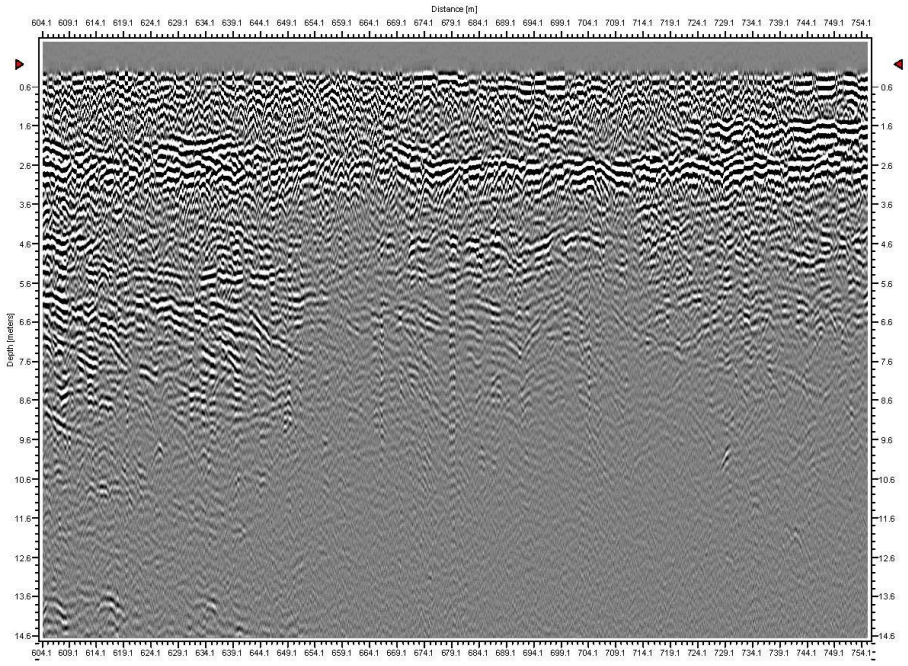

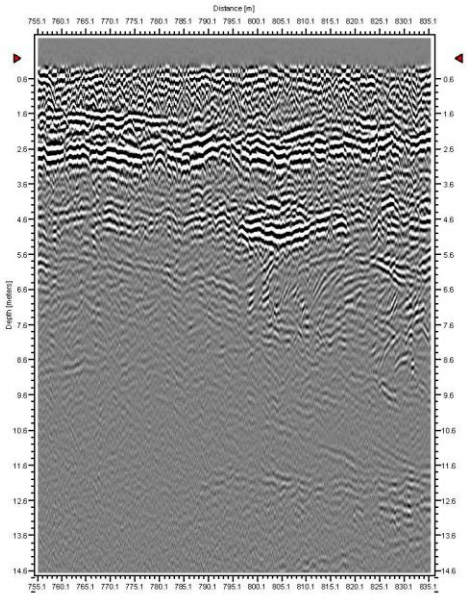

Profile 2 was run with the 250 MHz antenna going west to east from Junction 71 to 52. It has a distance of 835 meters and a depth of 14.6 meters. This profile features a strong distinction in the beginning of the clay layer at approximately 6 meters in depth.

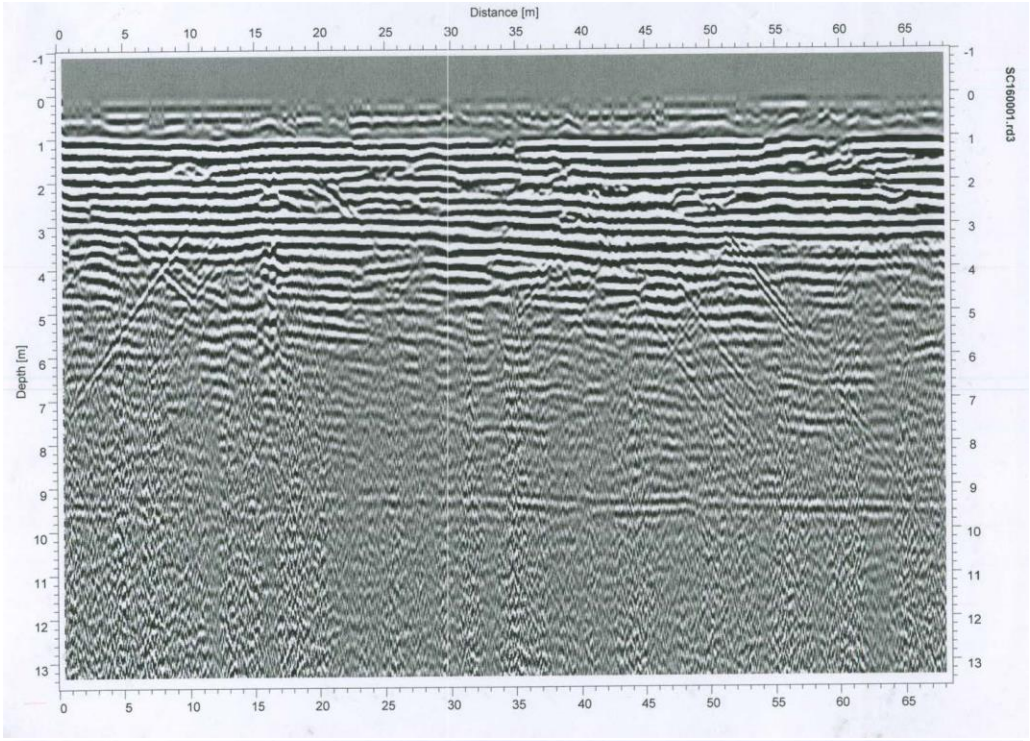
Distance [m]
0 5 10 15 20 25 30 35 40 45 50 55 60 65
Depth [m]
-1 0 1 2 3 4 5 6 7 8 9 10 11 12 13
SC160001.rd3

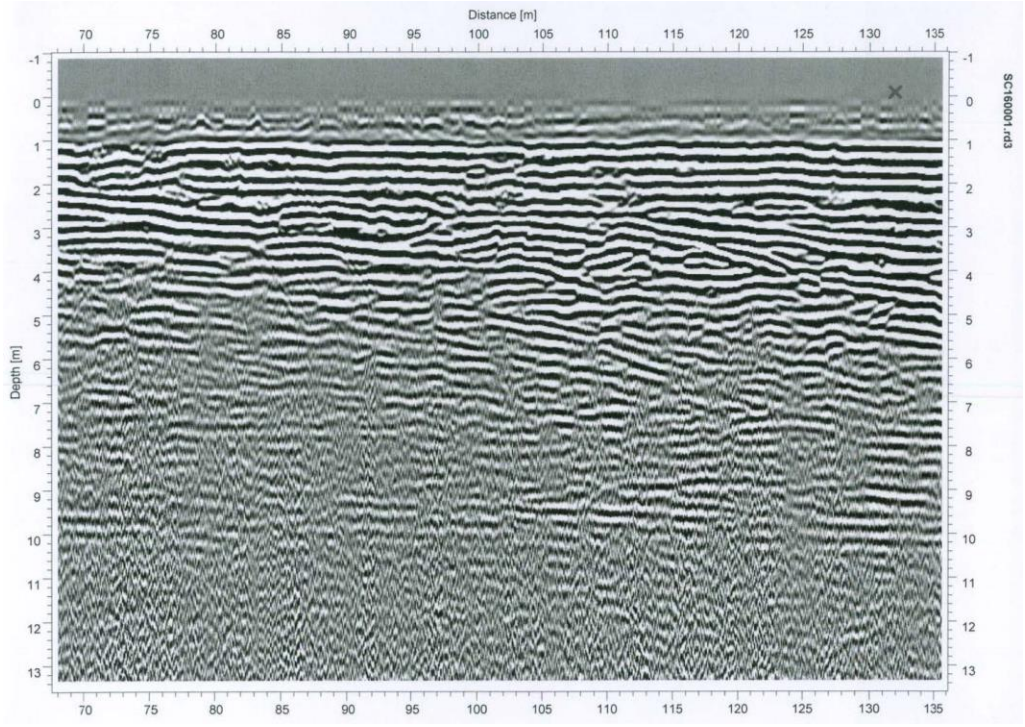
Distance [m]
70 75 80 85 90 95 100 105 110 115 120 125 130 135
Depth [m]
-1 0 1 2 3 4 5 6 7 8 9 10 11 12 13
SC160001.rd3

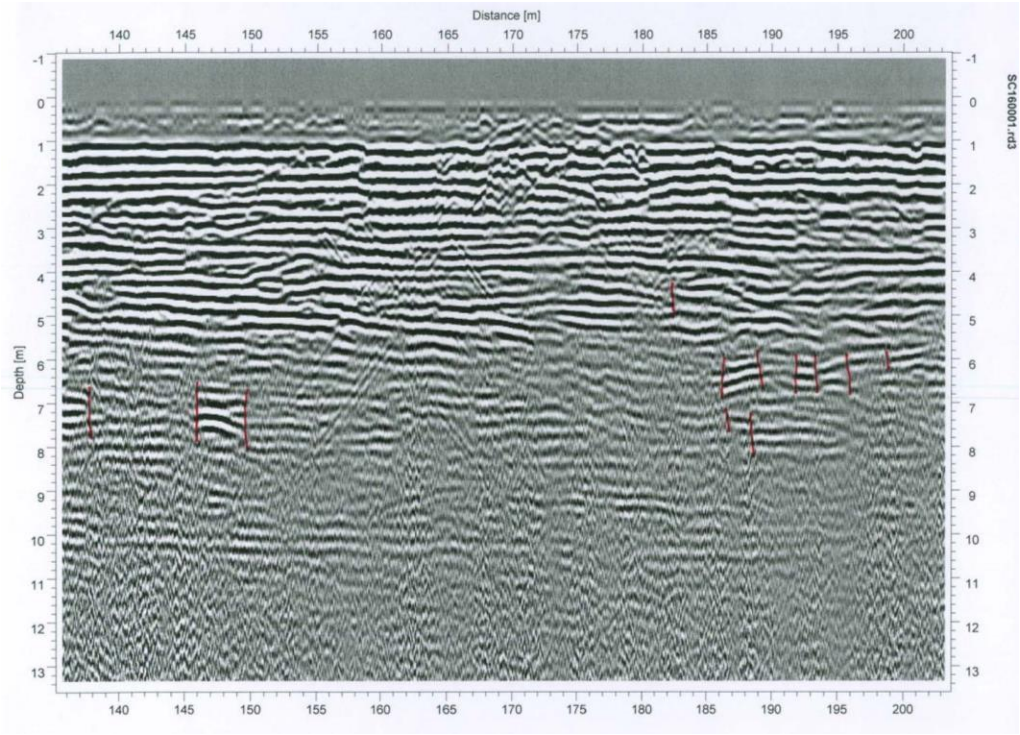
Distance [m]
140 145 150 155 160 165 170 175 180 185 190 195 200
Depth [m]
-1 0 1 2 3 4 5 6 7 8 9 10 11 12 13
SC160001.rd3

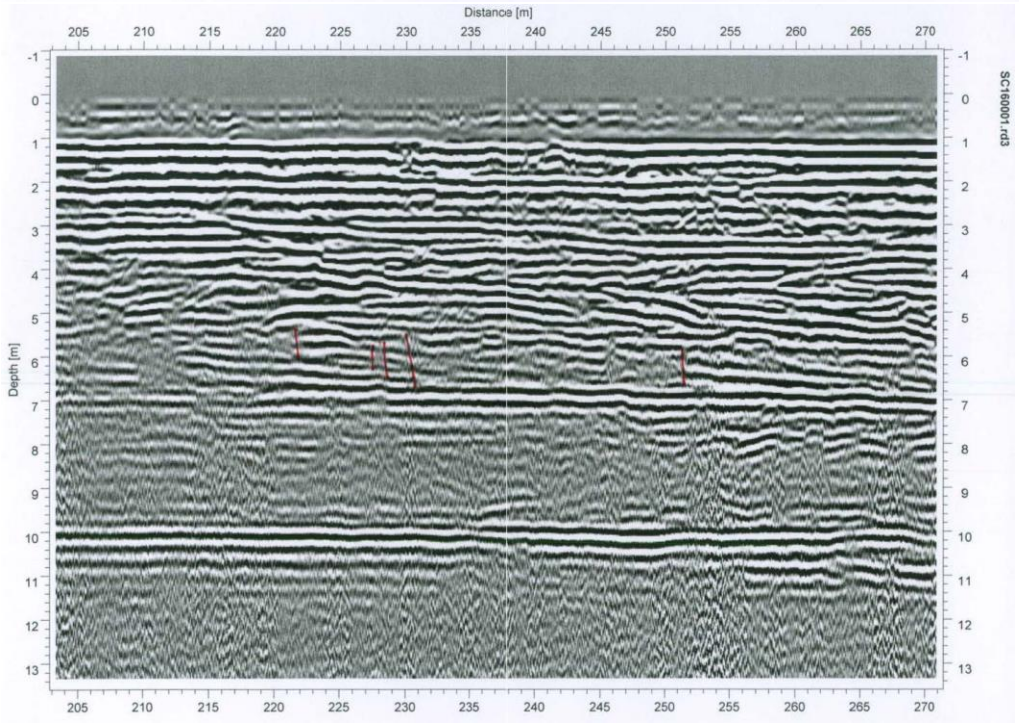
Distance [m]
205 210 215 220 225 230 235 240 245 250 255 260 265 270
Depth [m]
-1 0 1 2 3 4 5 6 7 8 9 10 11 12 13
SC160001.rd3

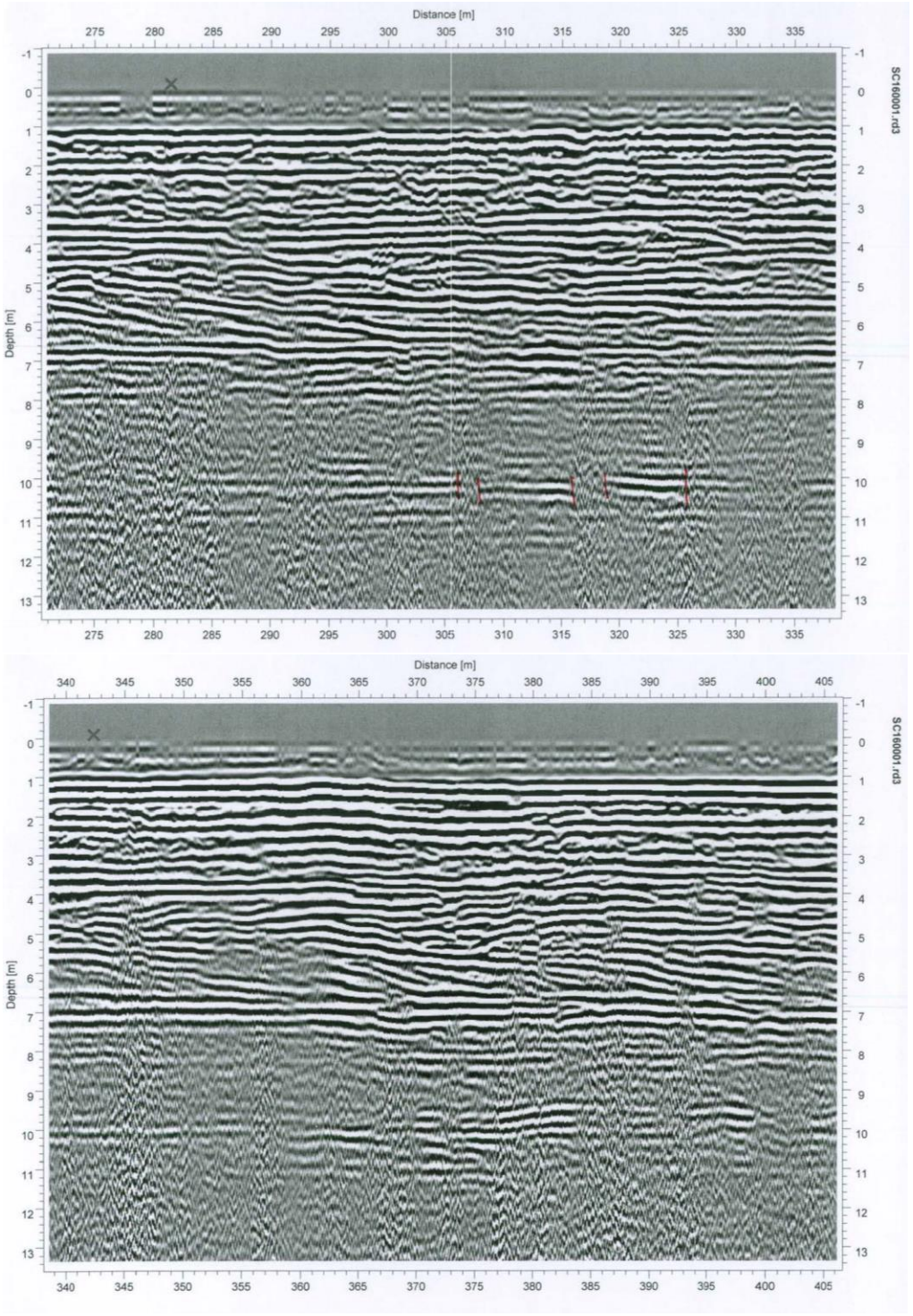
Distance [m]
275 280 285 290 295 300 305 310 315 320 325 330 335
Depth [m]
-1 0 1 2 3 4 5 6 7 8 9 10 11 12 13
SC160001.rd3
Distance [m]
340 345 350 355 360 365 370 375 380 385 390 395 400 405
Depth [m]
-1 0 1 2 3 4 5 6 7 8 9 10 11 12 13
SC160001.rd3

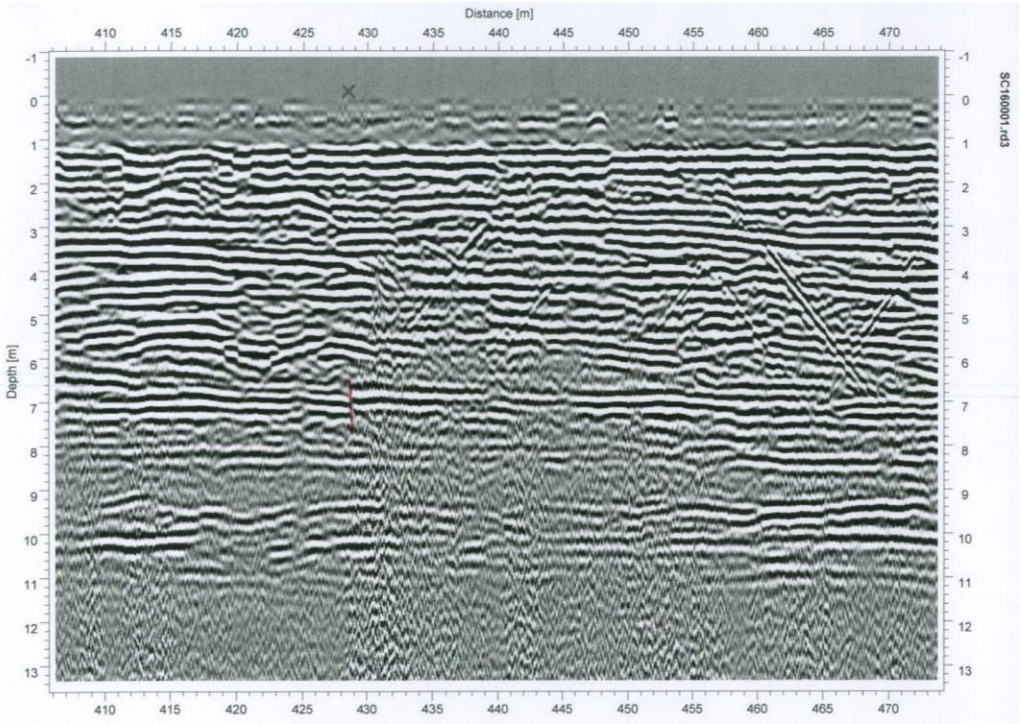
Distance [m]
410 415 420 425 430 435 440 445 450 455 460 465 470
Depth [m]
-1 0 1 2 3 4 5 6 7 8 9 10 11 12 13
SC160001.rd3

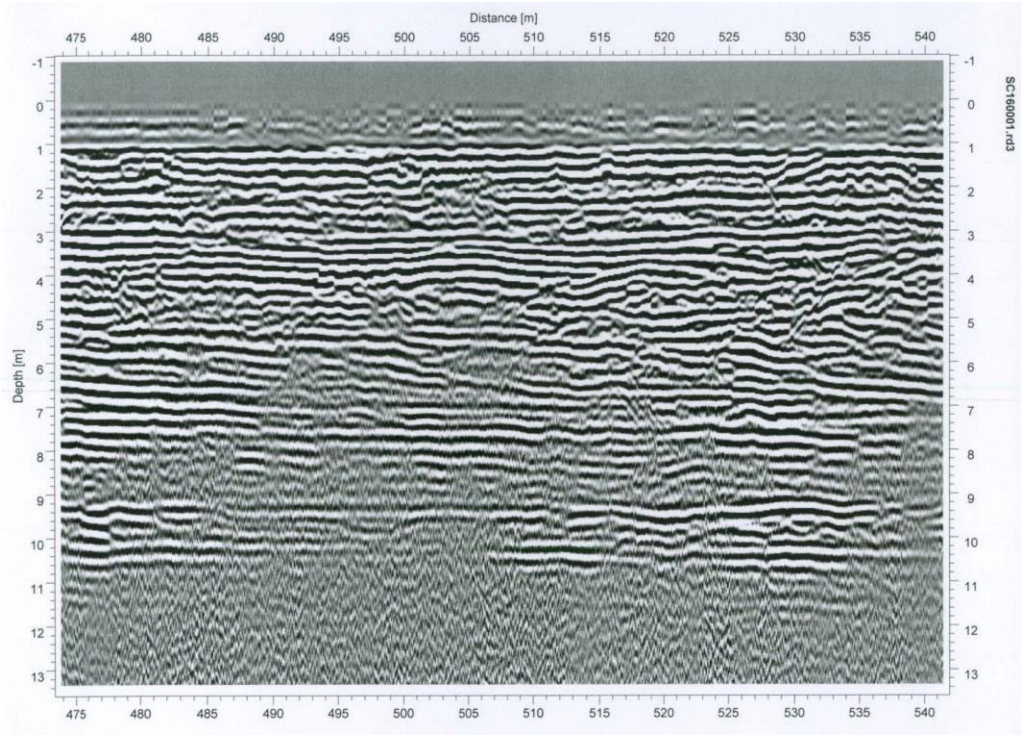
Distance [m]
475 480 485 490 495 500 505 510 515 520 525 530 535 540
Depth [m]
-1 0 1 2 3 4 5 6 7 8 9 10 11 12 13
SC160001.rd3

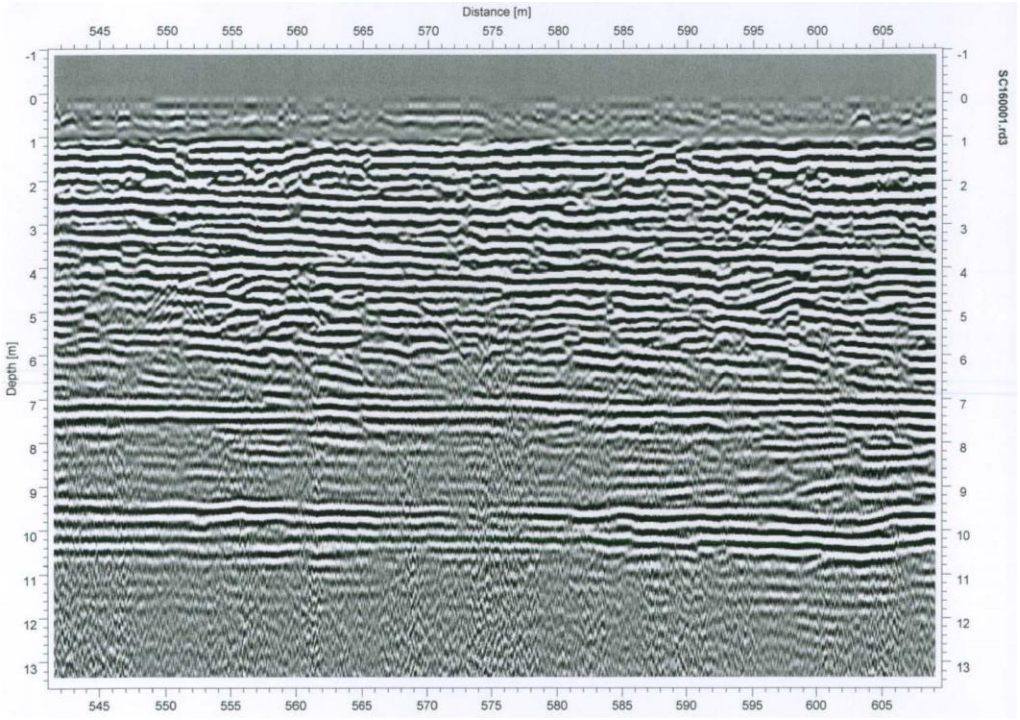
Distance [m]
545 550 555 560 565 570 575 580 585 590 595 600 605
Depth [m]
-1 0 1 2 3 4 5 6 7 8 9 10 11 12 13
SC160001.rd3

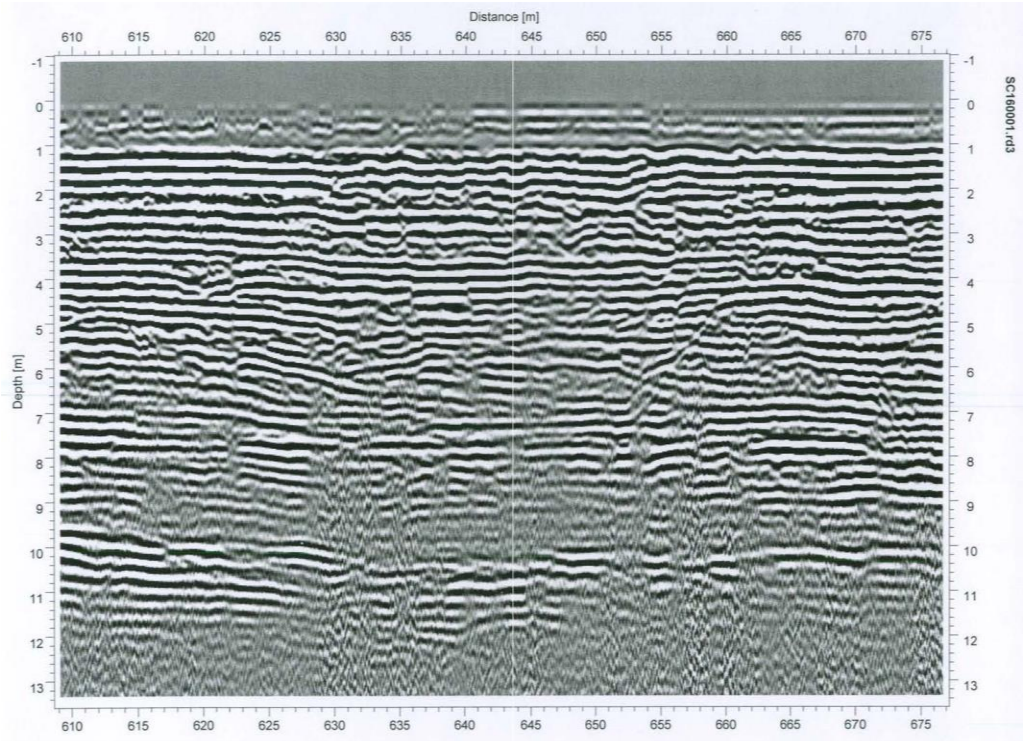
Distance [m]
610 615 620 625 630 635 640 645 650 655 660 665 670 675
Depth [m]
-1 0 1 2 3 4 5 6 7 8 9 10 11 12 13
SC160001.rd3

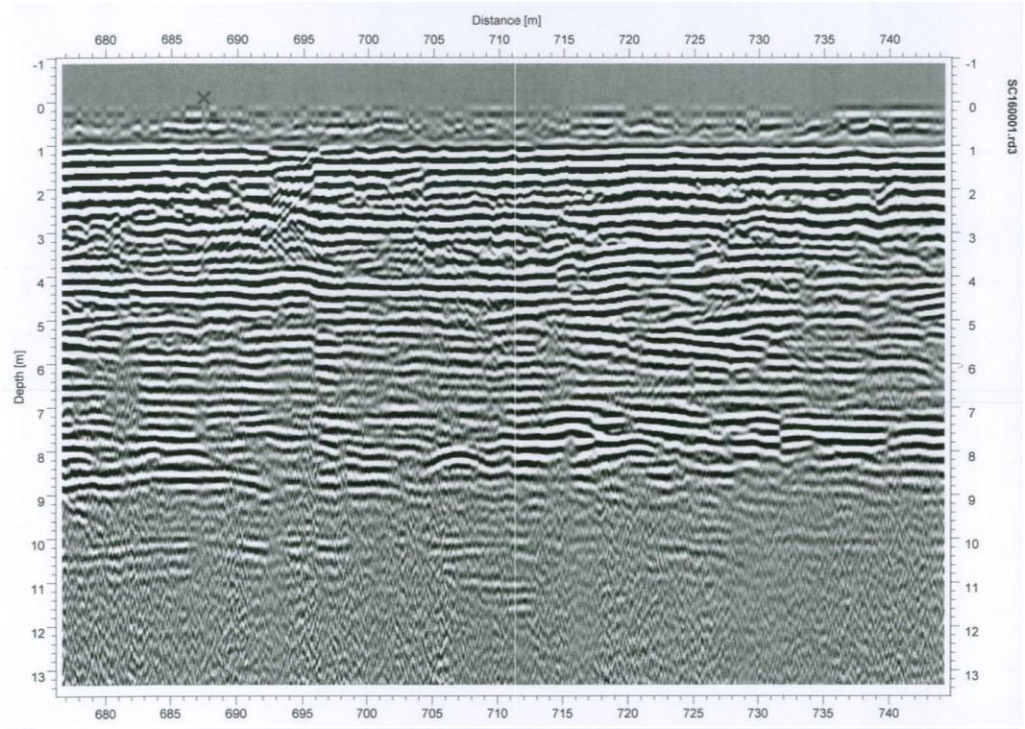
Distance [m]
680 685 690 695 700 705 710 715 720 725 730 735 740
Depth [m]
-1 0 1 2 3 4 5 6 7 8 9 10 11 12 13
SC160001.rd3

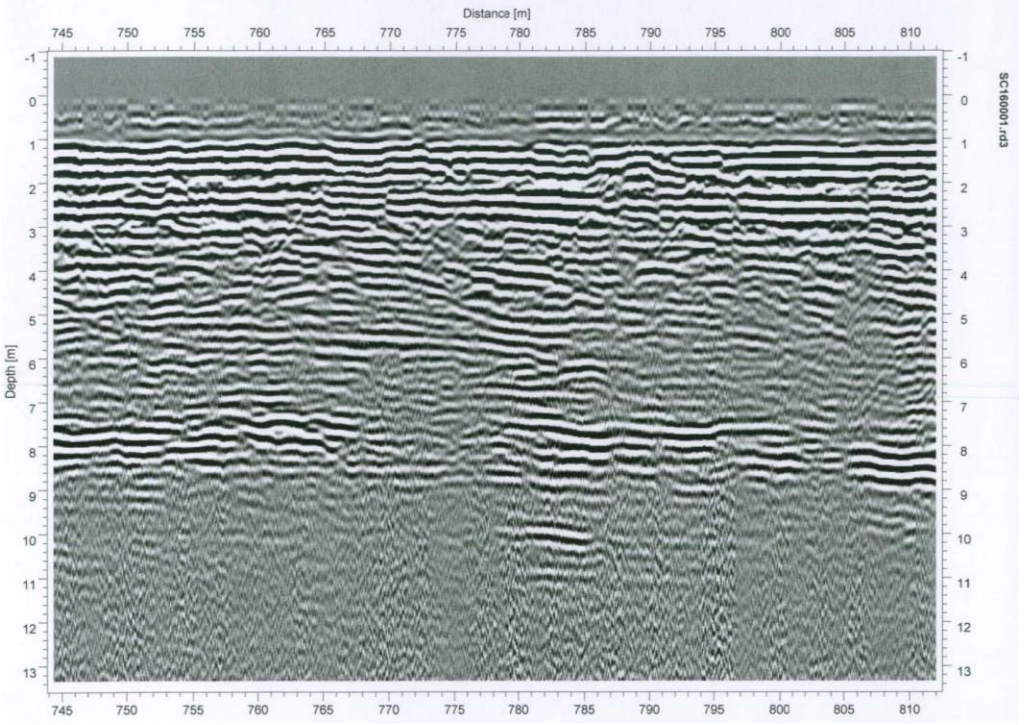
Distance [m]
745 750 755 760 765 770 775 780 785 790 795 800 805 810
Depth [m]
-1 0 1 2 3 4 5 6 7 8 9 10 11 12 13
SC160001.rd3

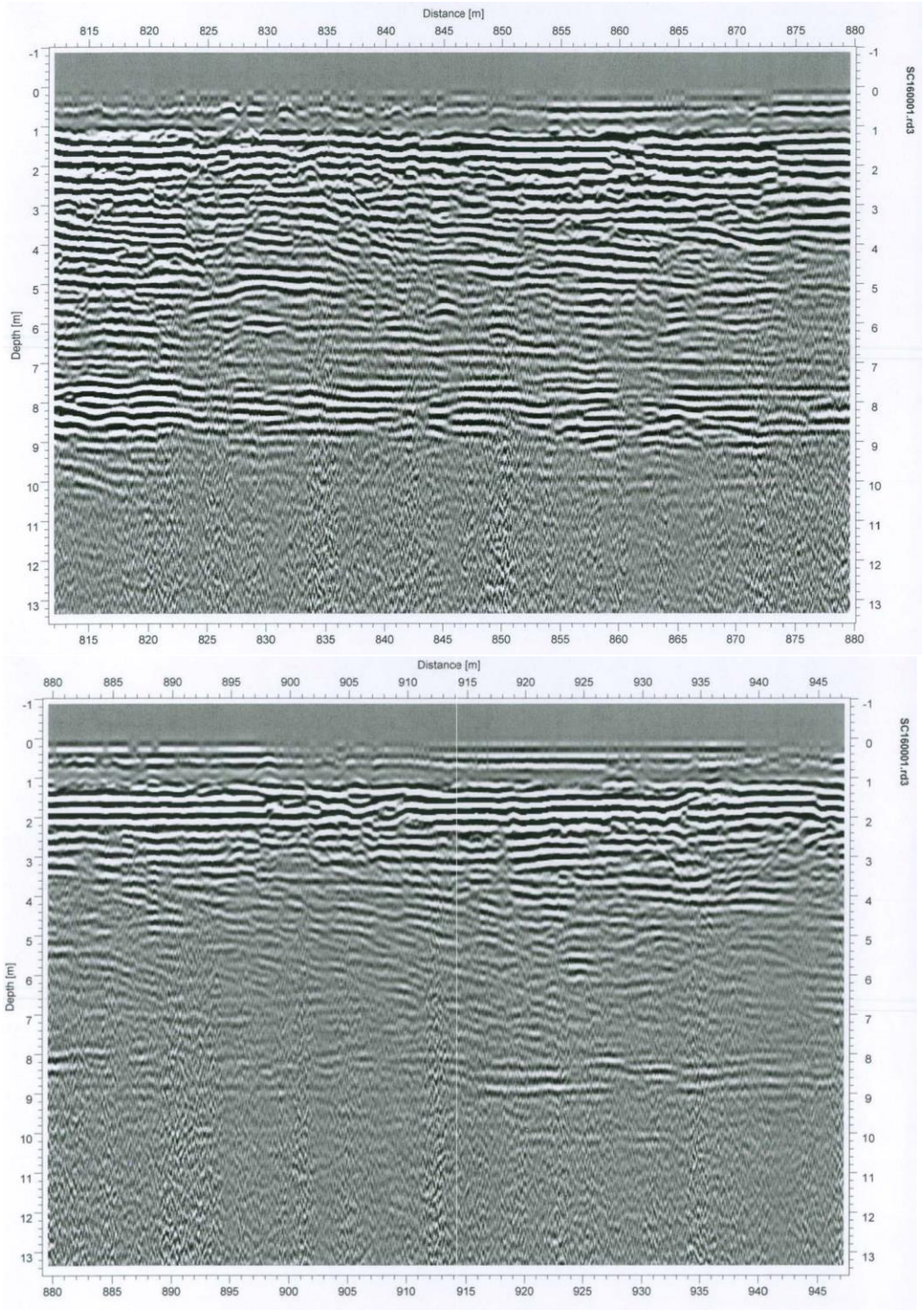
Distance [m]
815 820 825 830 835 840 845 850 855 860 865 870 875 880
Depth [m]
-1 0 1 2 3 4 5 6 7 8 9 10 11 12 13
SC160001.rd3
Distance [m]
880 885 890 895 900 905 910 915 920 925 930 935 940 945
Depth [m]
-1 0 1 2 3 4 5 6 7 8 9 10 11 12 13
SC160001.rd3

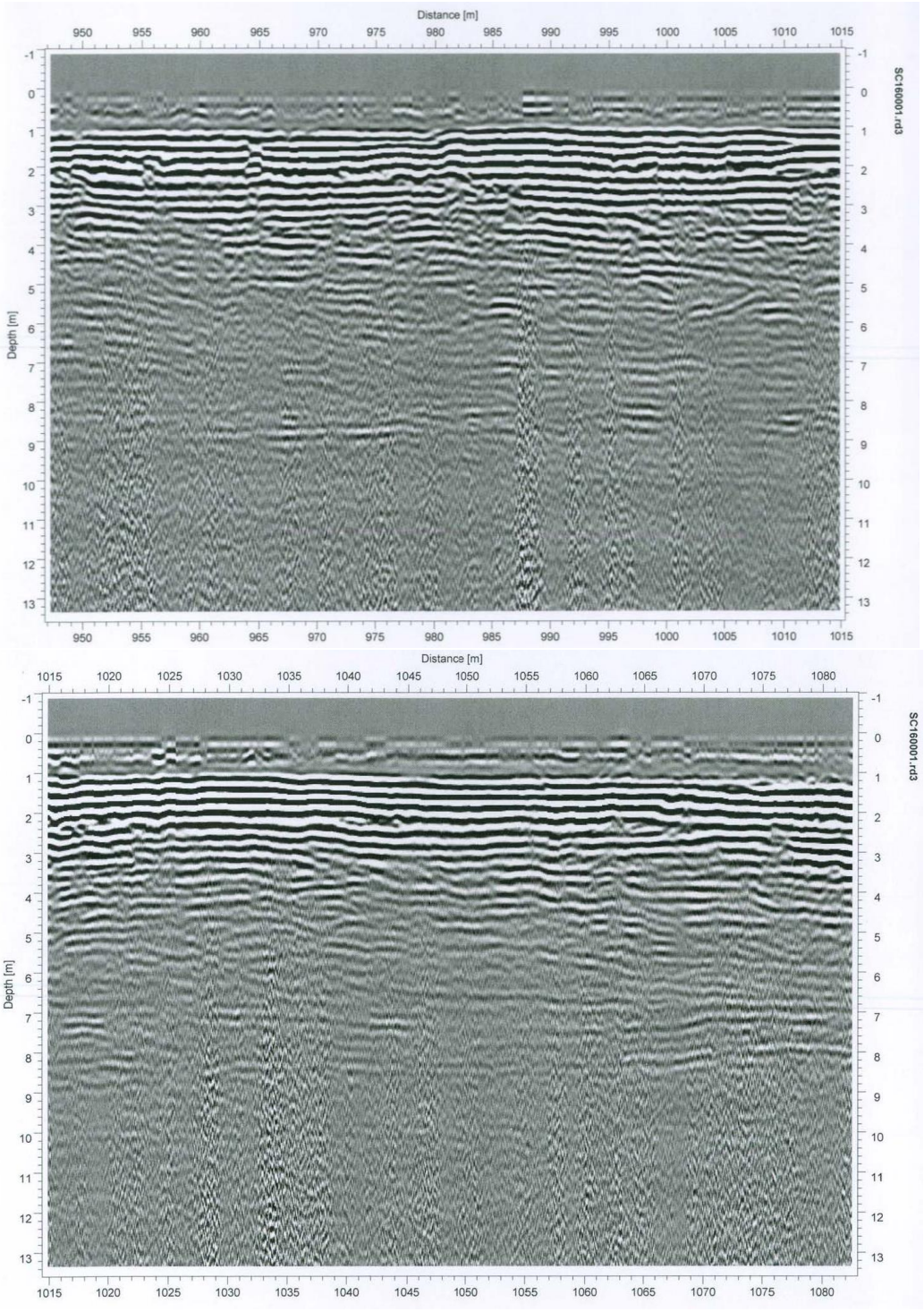
Distance [m]
950 955 960 965 970 975 980 985 990 995 1000 1005 1010 1015
Depth [m]
-1 0 1 2 3 4 5 6 7 8 9 10 11 12 13
SC160001.rd3
Distance [m]
1015 1020 1025 1030 1035 1040 1045 1050 1055 1060 1065 1070 1075 1080
Depth [m]
-1 0 1 2 3 4 5 6 7 8 9 10 11 12 13
SC160001.rd3

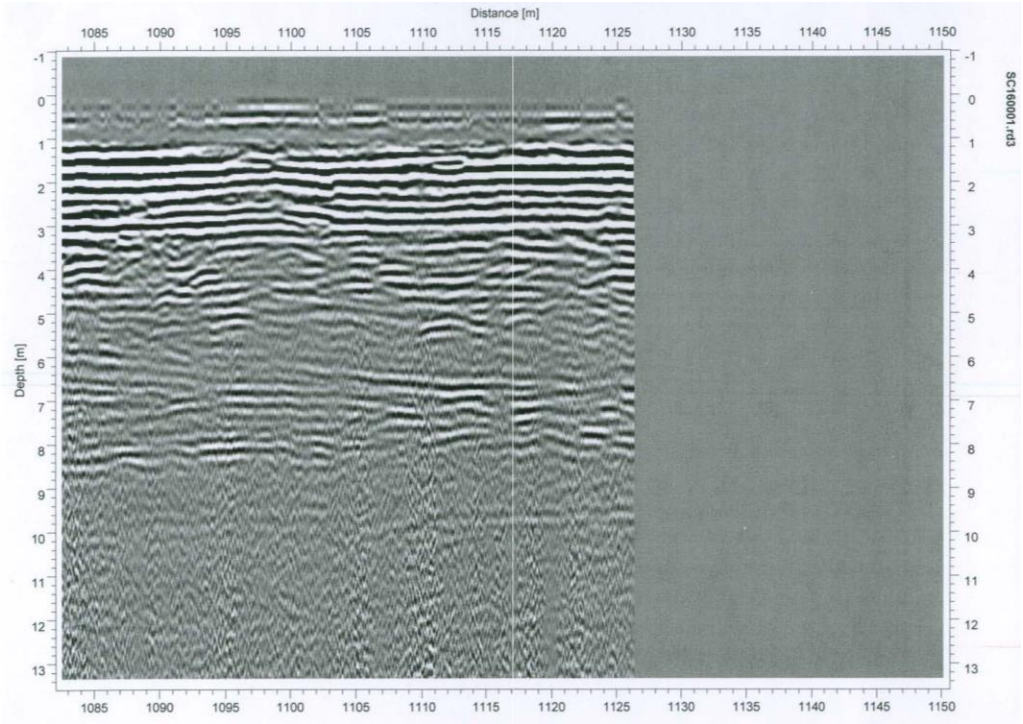

Profile 3 was run using the 100 MHz antenna going west to east from Junction 71 to 52 to 26. It has a distance of 1126 meters and a depth of approximately 13.4 meters. This profile exhibits fairly strong attenuation throughout and shows changes in stratigraphy especially in images 4-10.

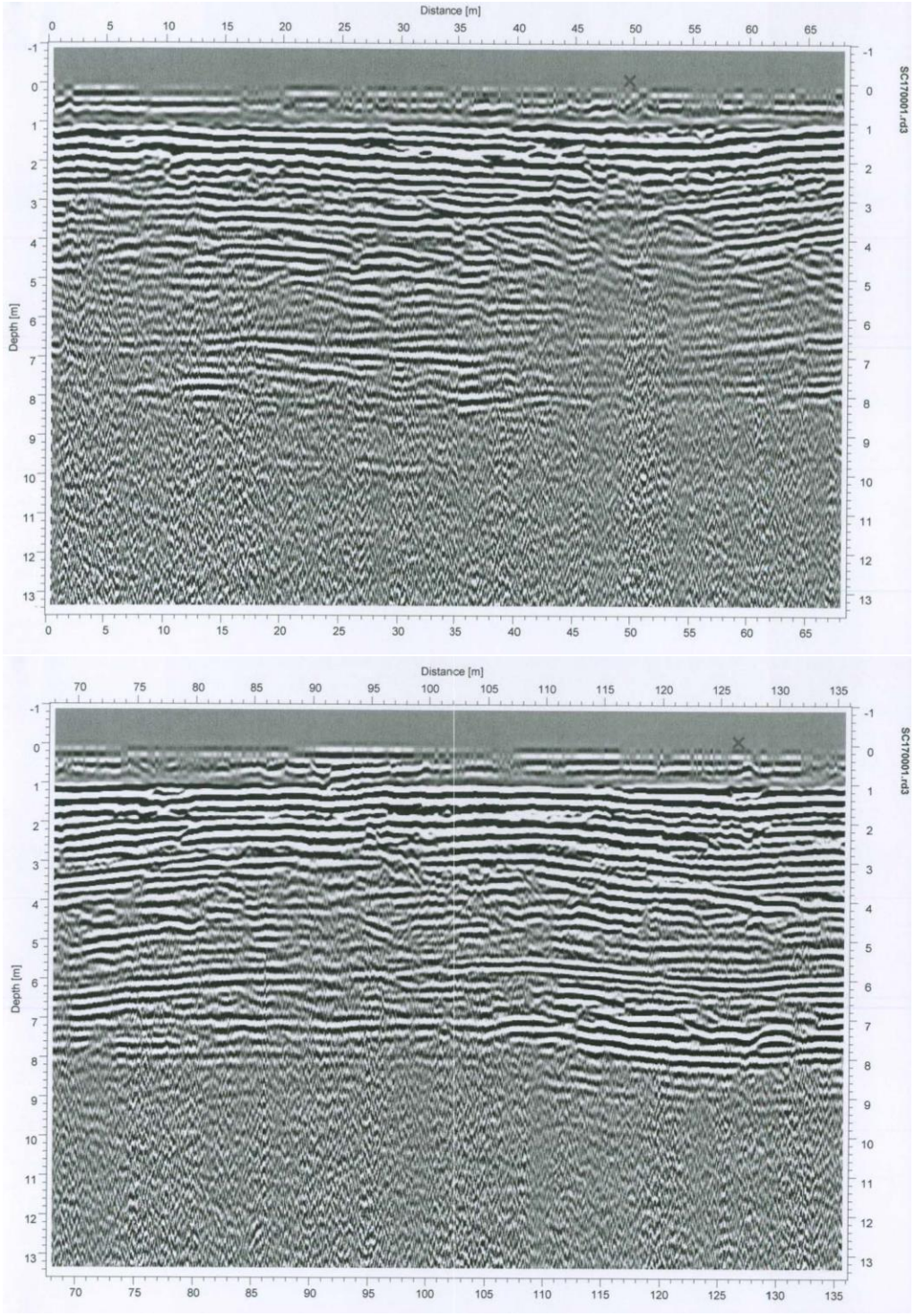
Distance [m]
Depth [m]
SC170001.rd3
Distance [m]
Depth [m]
SC170001.rd3

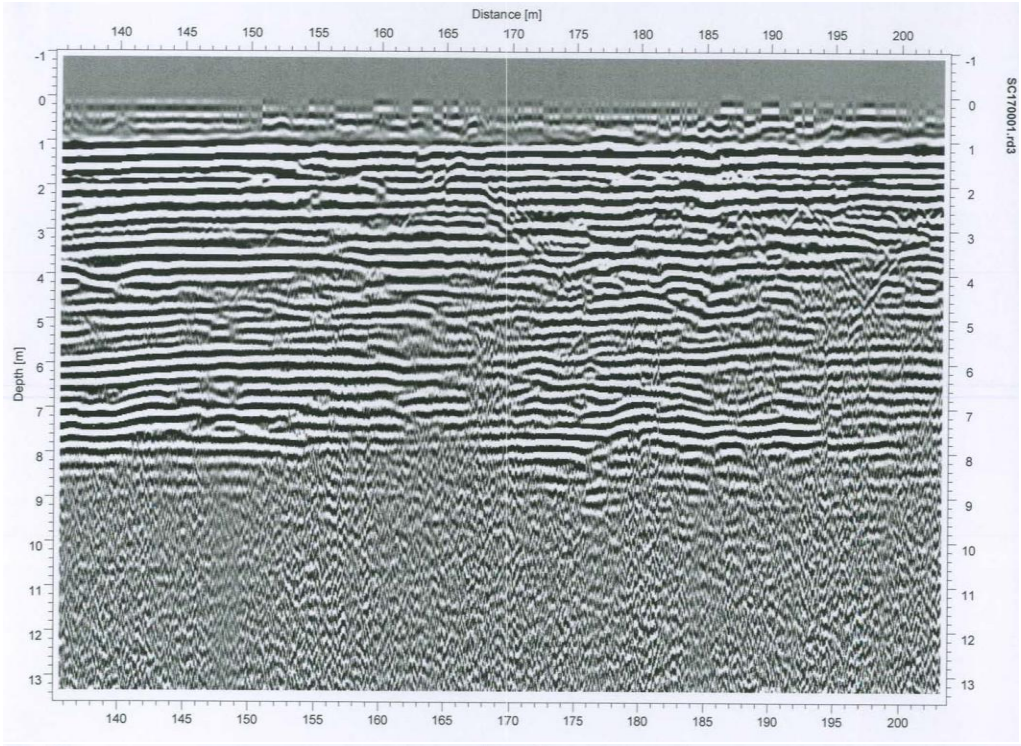
Distance [m]
140 145 150 155 160 165 170 175 180 185 190 195 200
Depth [m]
-1 0 1 2 3 4 5 6 7 8 9 10 11 12 13
SC170001.rd3

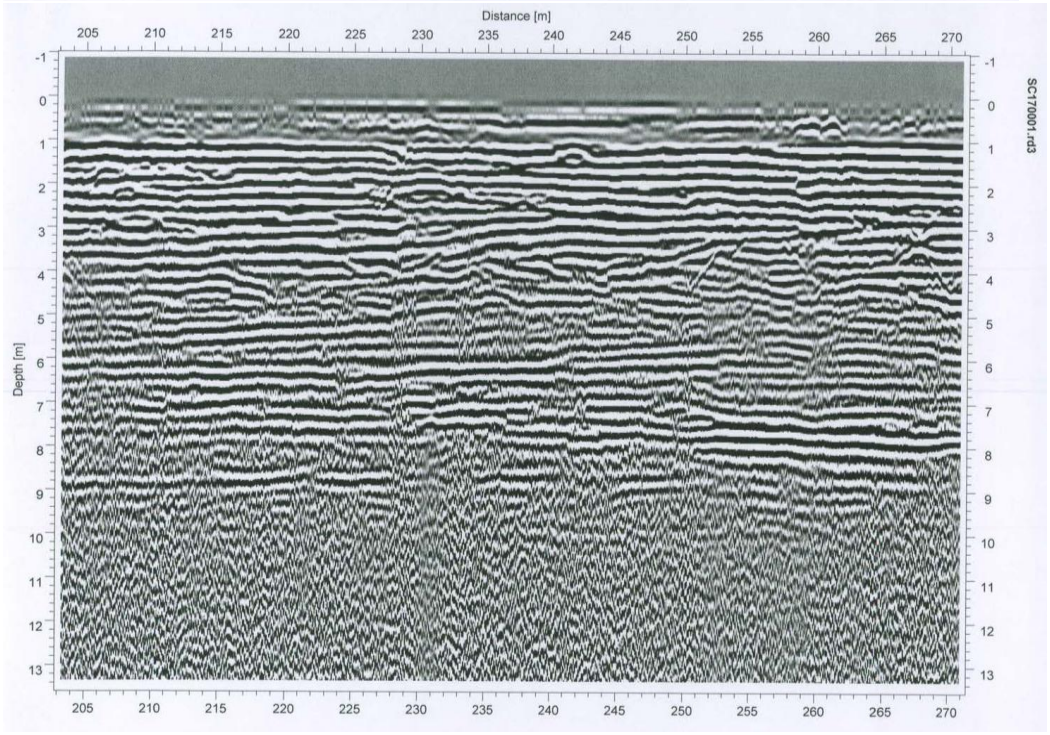
Distance [m]
205 210 215 220 225 230 235 240 245 250 255 260 265 270
Depth [m]
-1 0 1 2 3 4 5 6 7 8 9 10 11 12 13
SC170001.rd3

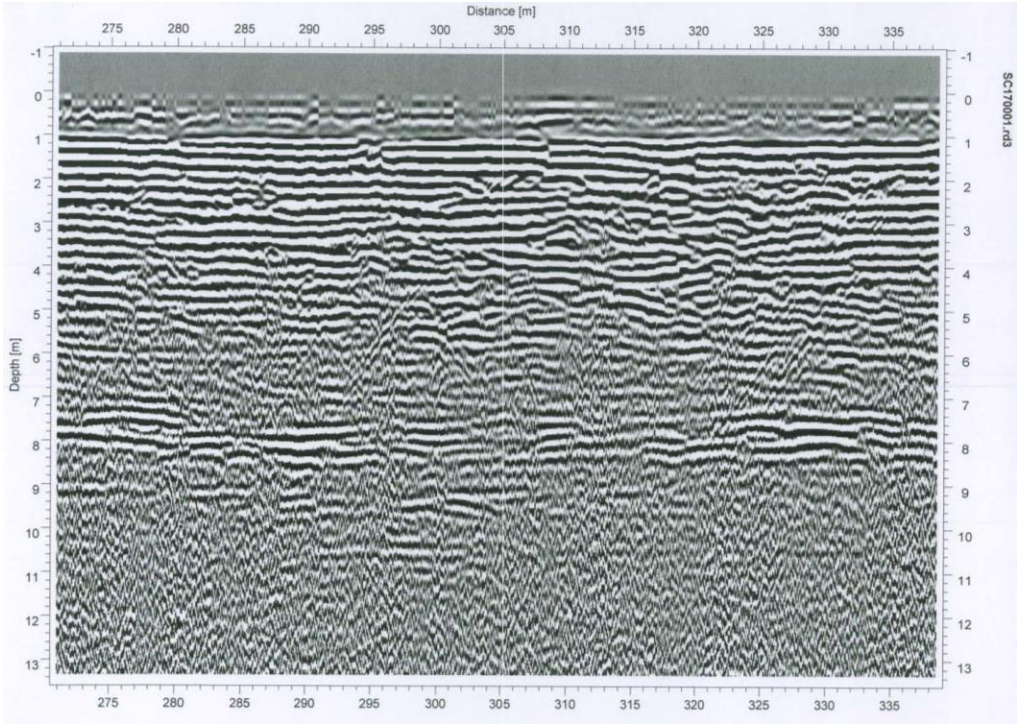
Distance [m]
275 280 285 290 295 300 305 310 315 320 325 330 335
Depth [m]
-1 0 1 2 3 4 5 6 7 8 9 10 11 12 13
SC170001.rd3

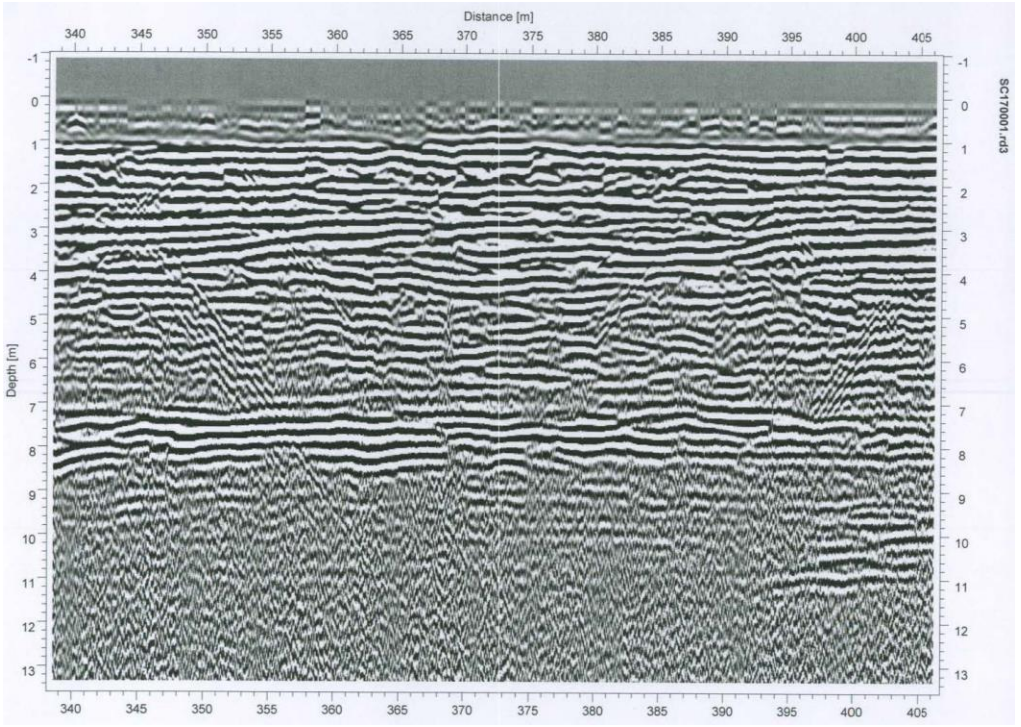
Distance [m]
340 345 350 355 360 365 370 375 380 385 390 395 400 405
Depth [m]
-1 0 1 2 3 4 5 6 7 8 9 10 11 12 13
SC170001.rd3

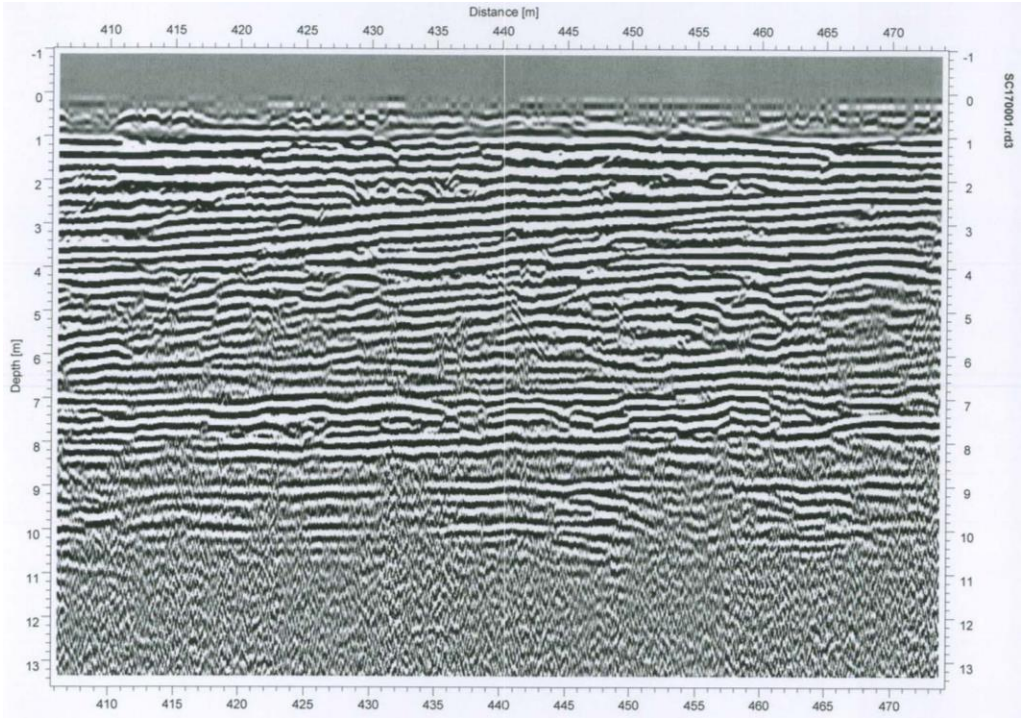
Distance [m]
410 415 420 425 430 435 440 445 450 455 460 465 470
Depth [m]
-1 0 1 2 3 4 5 6 7 8 9 10 11 12 13
SC170001.rd3

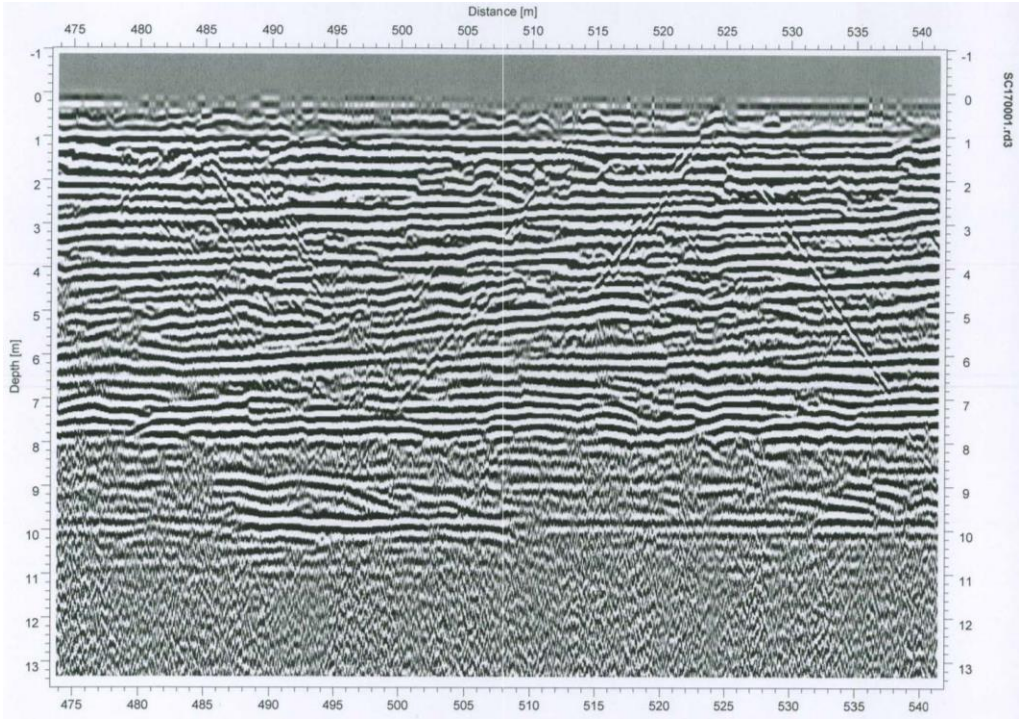
Distance [m]
475 480 485 490 495 500 505 510 515 520 525 530 535 540
Depth [m]
-1 0 1 2 3 4 5 6 7 8 9 10 11 12 13
SC170001.rd3

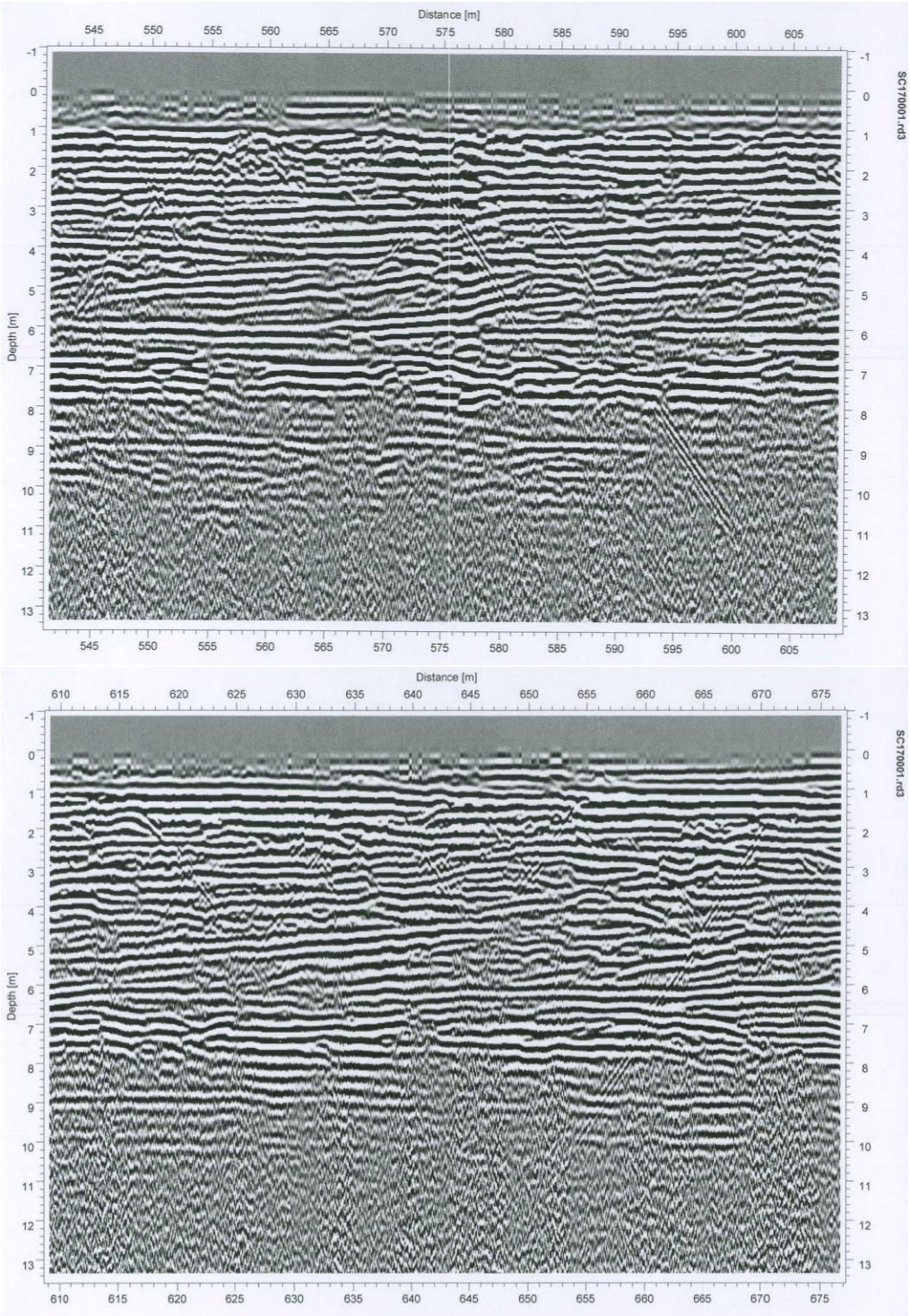
Distance [m]
545 550 555 560 565 570 575 580 585 590 595 600 605
Depth [m]
-1 0 1 2 3 4 5 6 7 8 9 10 11 12 13
SC170001.rd3
Distance [m]
610 615 620 625 630 635 640 645 650 655 660 665 670 675
Depth [m]
-1 0 1 2 3 4 5 6 7 8 9 10 11 12 13
SC170001.rd3

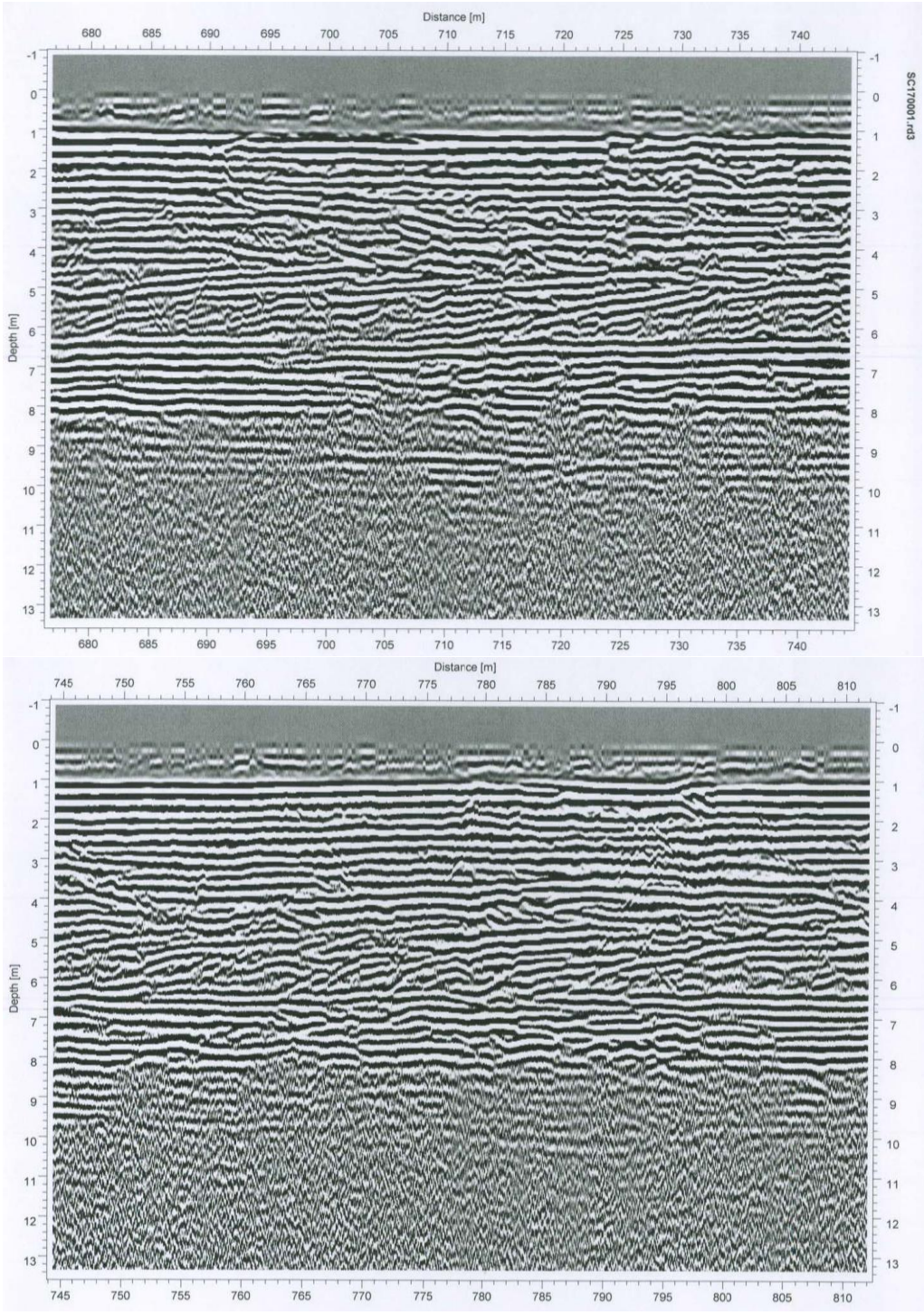
Distance [m]
680 685 690 695 700 705 710 715 720 725 730 735 740
Depth [m]
-1 0 1 2 3 4 5 6 7 8 9 10 11 12 13
SC170001.rd3
Distance [m]
745 750 755 760 765 770 775 780 785 790 795 800 805 810
Depth [m]
-1 0 1 2 3 4 5 6 7 8 9 10 11 12 13
SC170001.rd3

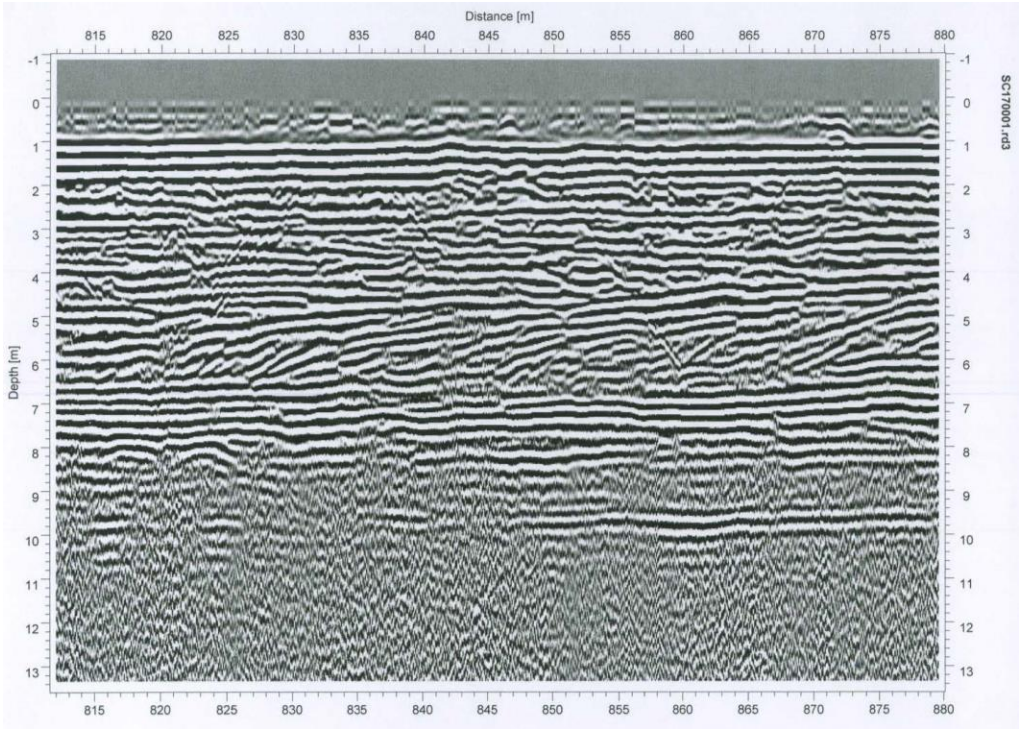
Distance [m]
815 820 825 830 835 840 845 850 855 860 865 870 875 880
Depth [m]
-1 0 1 2 3 4 5 6 7 8 9 10 11 12 13
SC170001.rd3

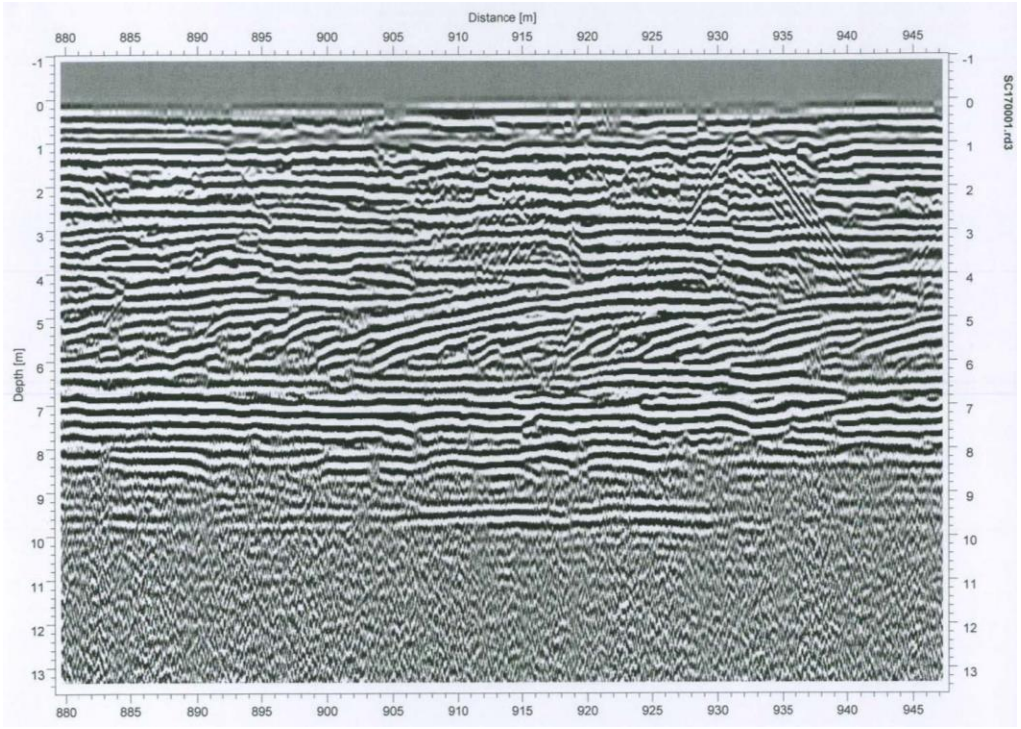
Distance [m]
880 885 890 895 900 905 910 915 920 925 930 935 940 945
Depth [m]
-1 0 1 2 3 4 5 6 7 8 9 10 11 12 13
SC170001.rd3

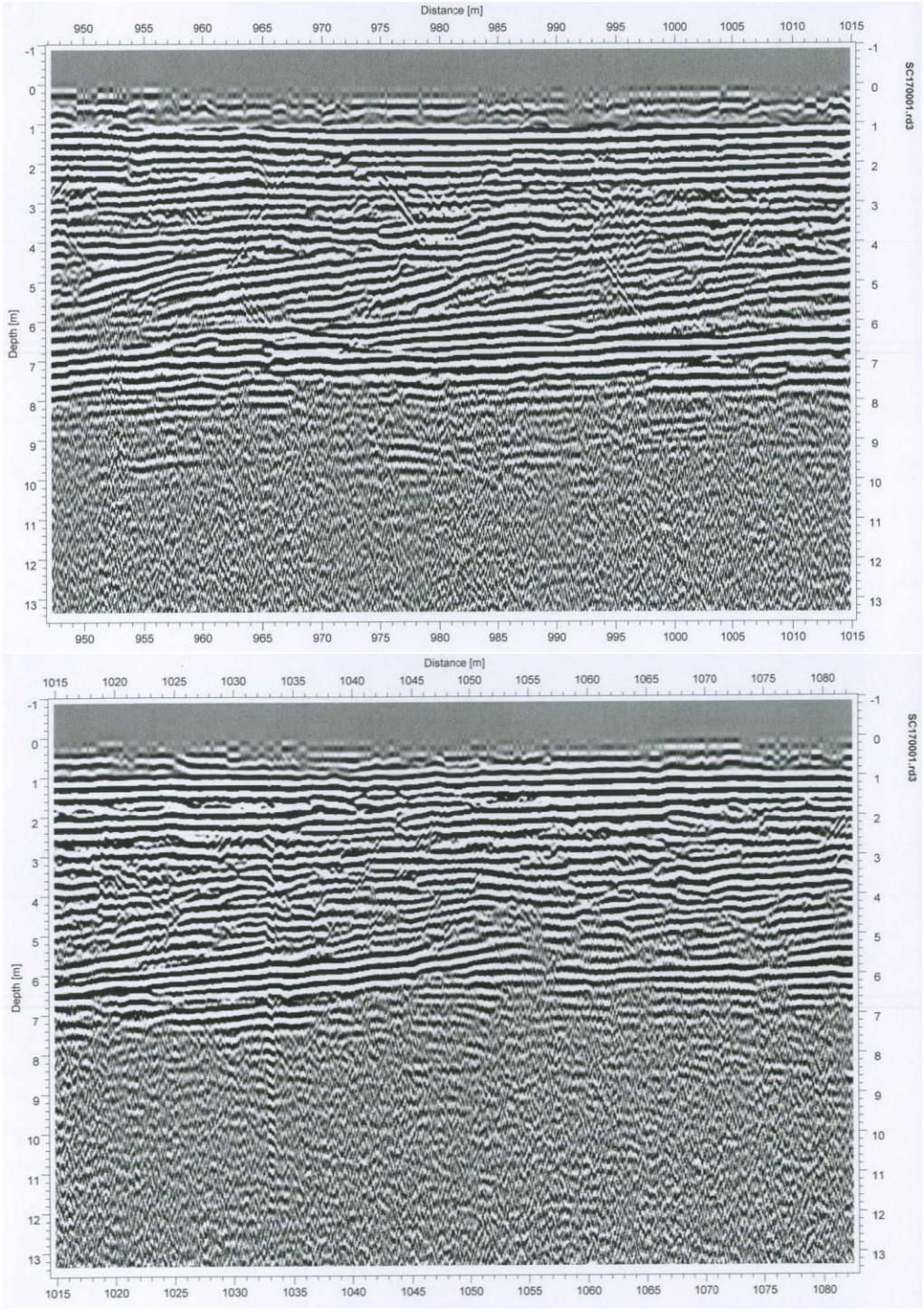
Distance [m]
950 955 960 965 970 975 980 985 990 995 1000 1005 1010 1015
Depth [m]
-1 0 1 2 3 4 5 6 7 8 9 10 11 12 13
SC170001.rd3
Distance [m]
1015 1020 1025 1030 1035 1040 1045 1050 1055 1060 1065 1070 1075 1080
Depth [m]
-1 0 1 2 3 4 5 6 7 8 9 10 11 12 13
SC170001.rd3

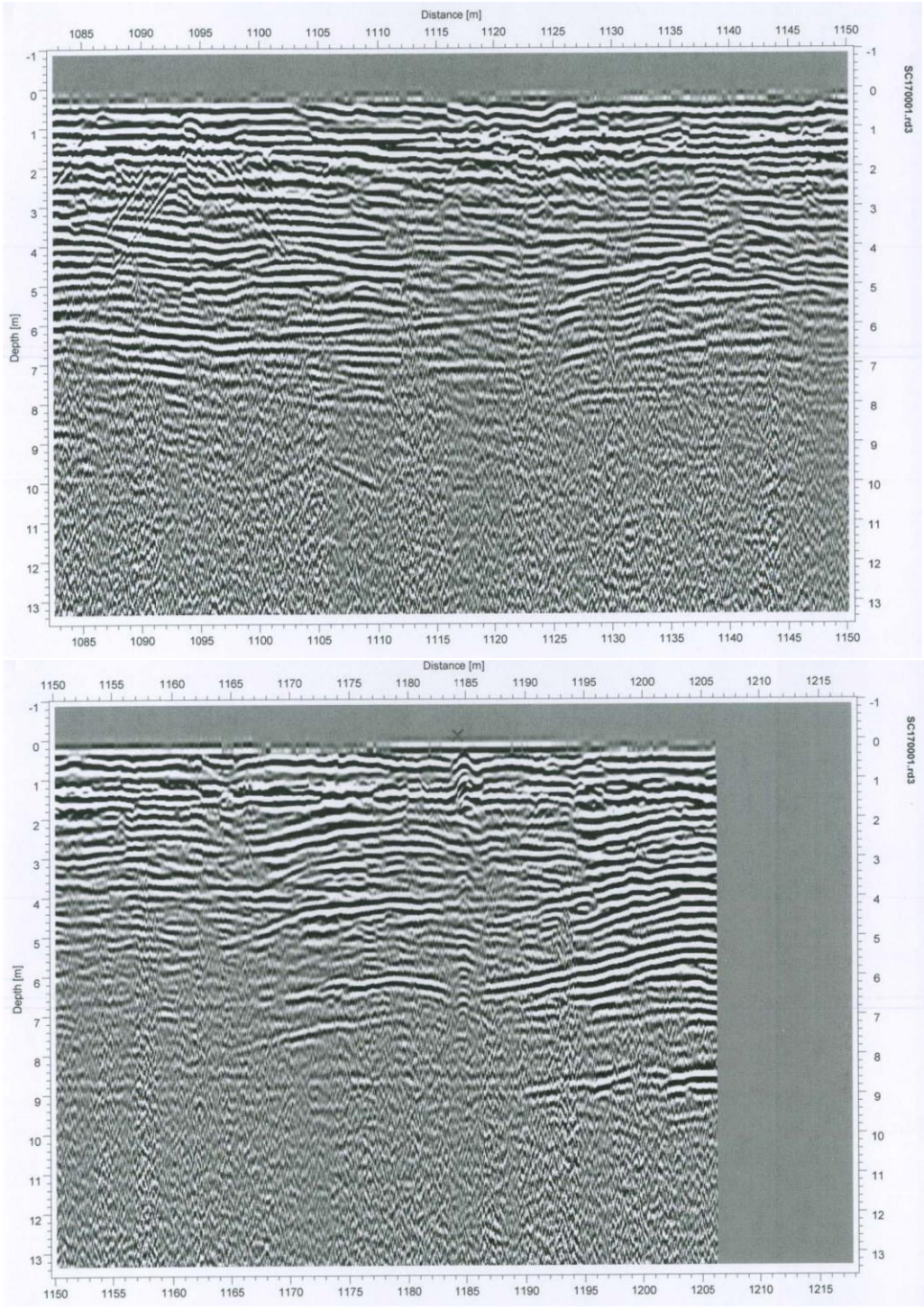

Profile 4 was run with the 100 MHz antenna going fron Junction 26 north to Junction 24. It is approximately 1206 meters in distance and 13.4 meters in depth. This profile shows multitudes of fractures, a possible angular unconformity around 6 meters in depth, and strong attenuation starting at about 9 meters in depth. Excerpts of this profile are used in the results section.

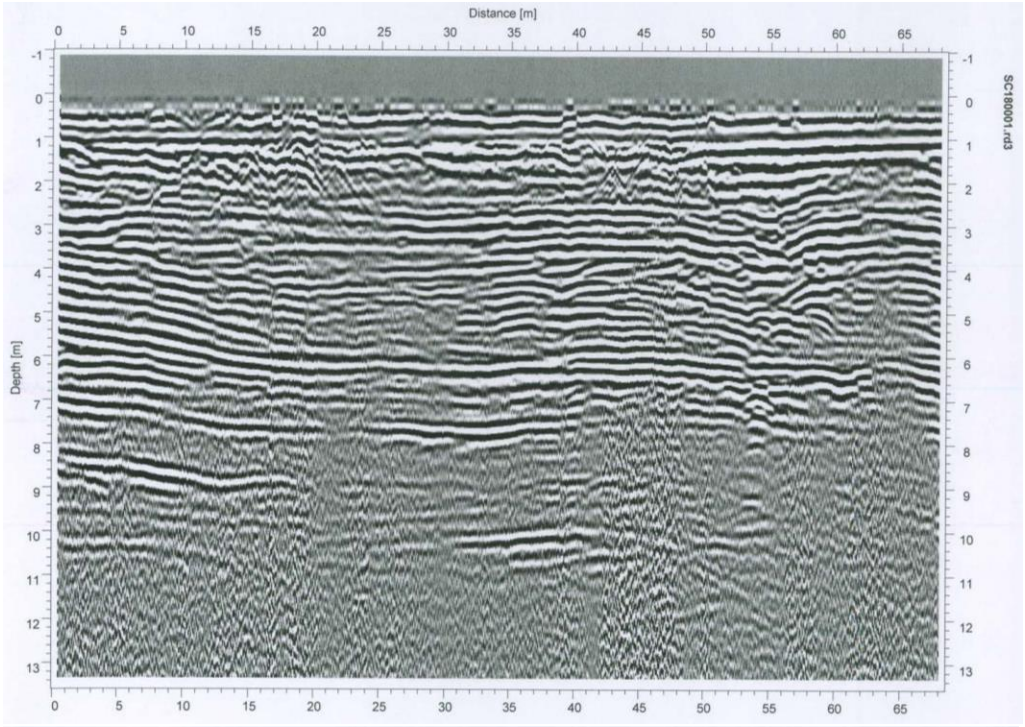
Distance [m]
0 5 10 15 20 25 30 35 40 45 50 55 60 65
Depth [m]
-1 0 1 2 3 4 5 6 7 8 9 10 11 12 13
SC180001.rd3

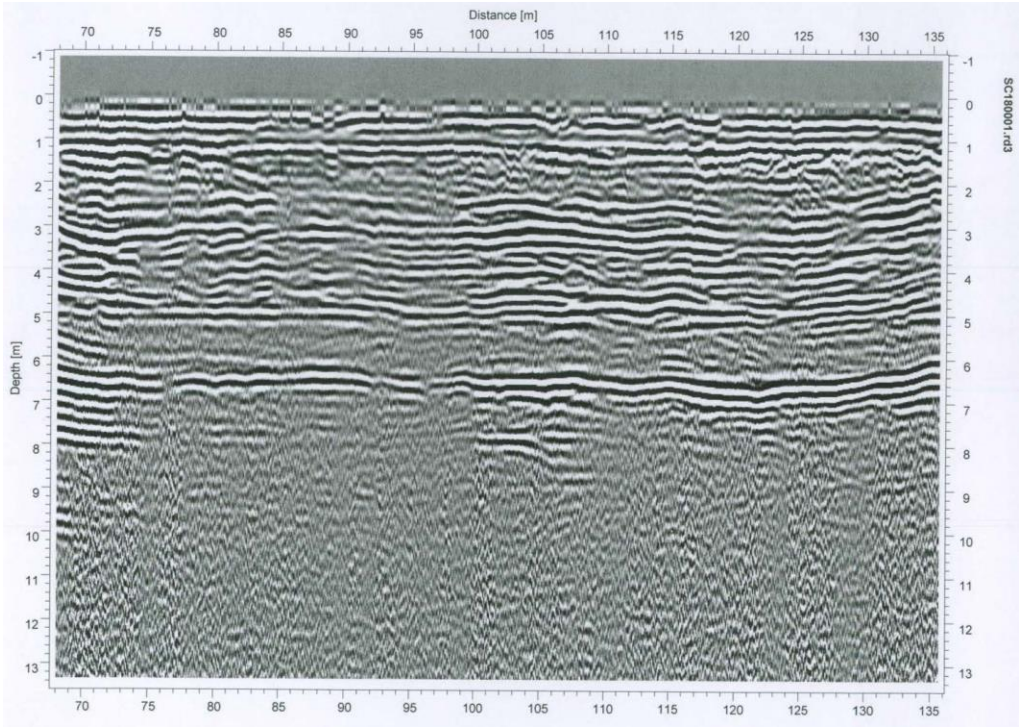
Distance [m]
70 75 80 85 90 95 100 105 110 115 120 125 130 135
Depth [m]
-1 0 1 2 3 4 5 6 7 8 9 10 11 12 13
SC180001.rd3

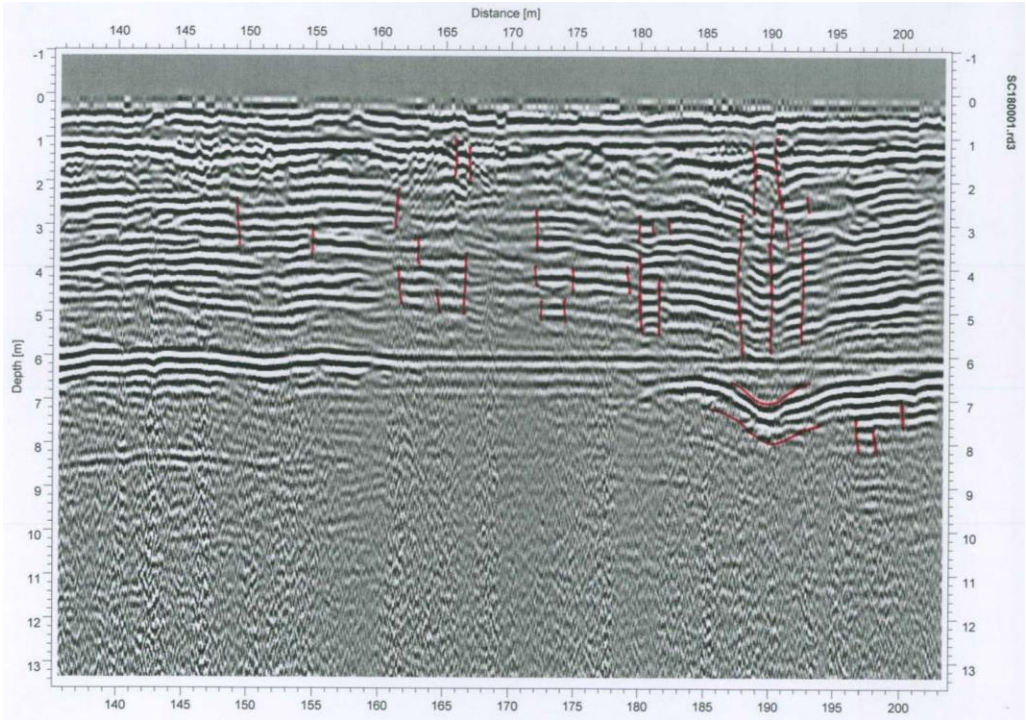
Distance [m]
140 145 150 155 160 165 170 175 180 185 190 195 200
Depth [m]
-1 0 1 2 3 4 5 6 7 8 9 10 11 12 13
SC180001.rd3

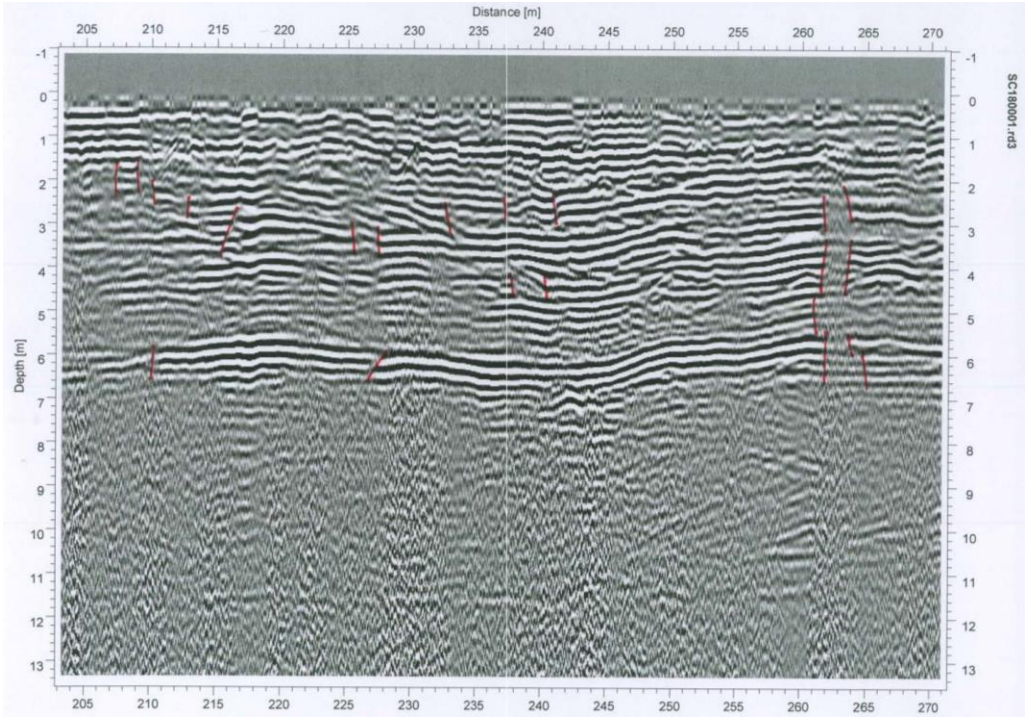
Distance [m]
205 210 215 220 225 230 235 240 245 250 255 260 265 270
Depth [m]
-1 0 1 2 3 4 5 6 7 8 9 10 11 12 13
SC180001.rd3

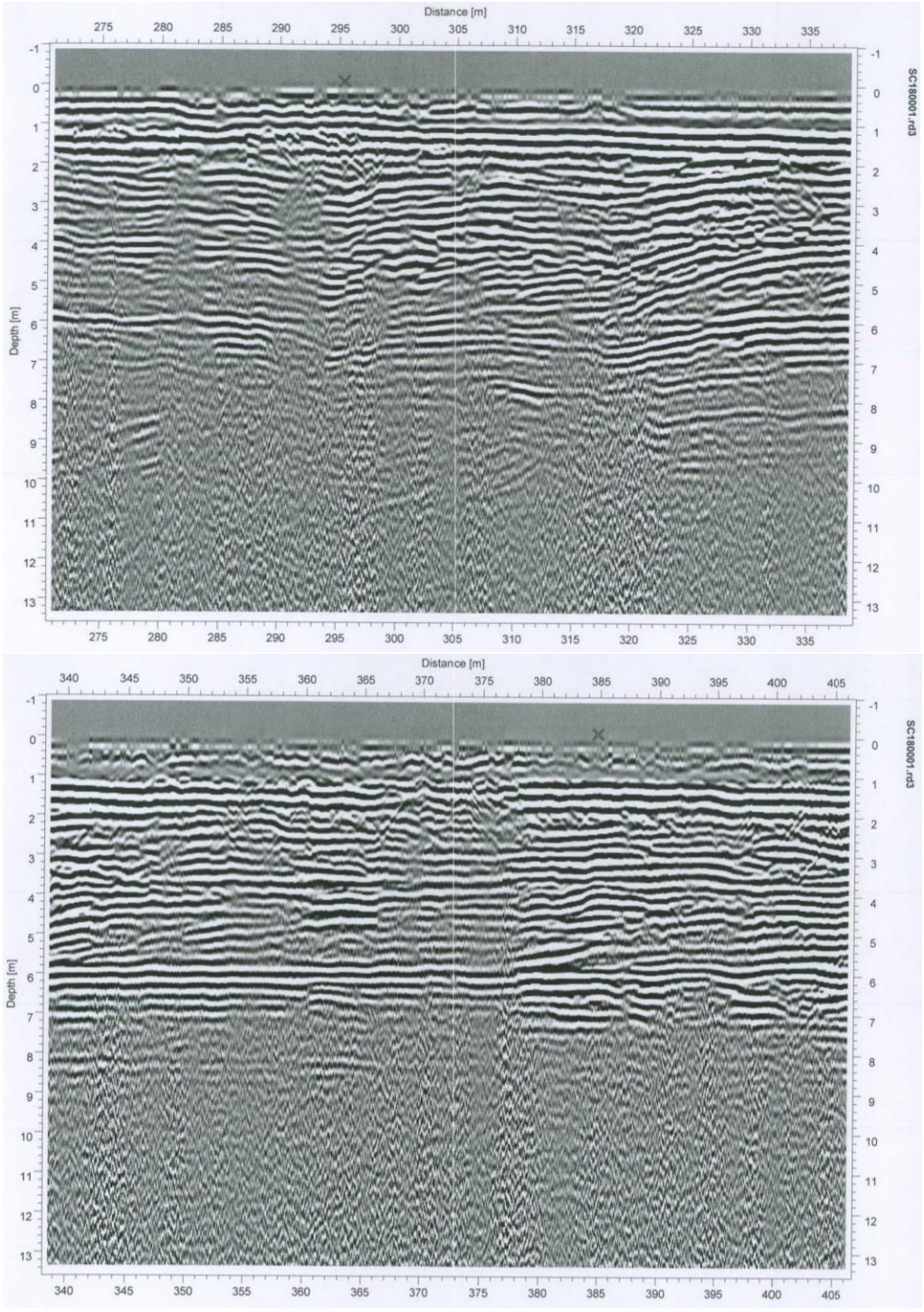
Distance [m]
Depth [m]
SC180001.rd3
Distance [m]
Depth [m]
SC180001.rd3

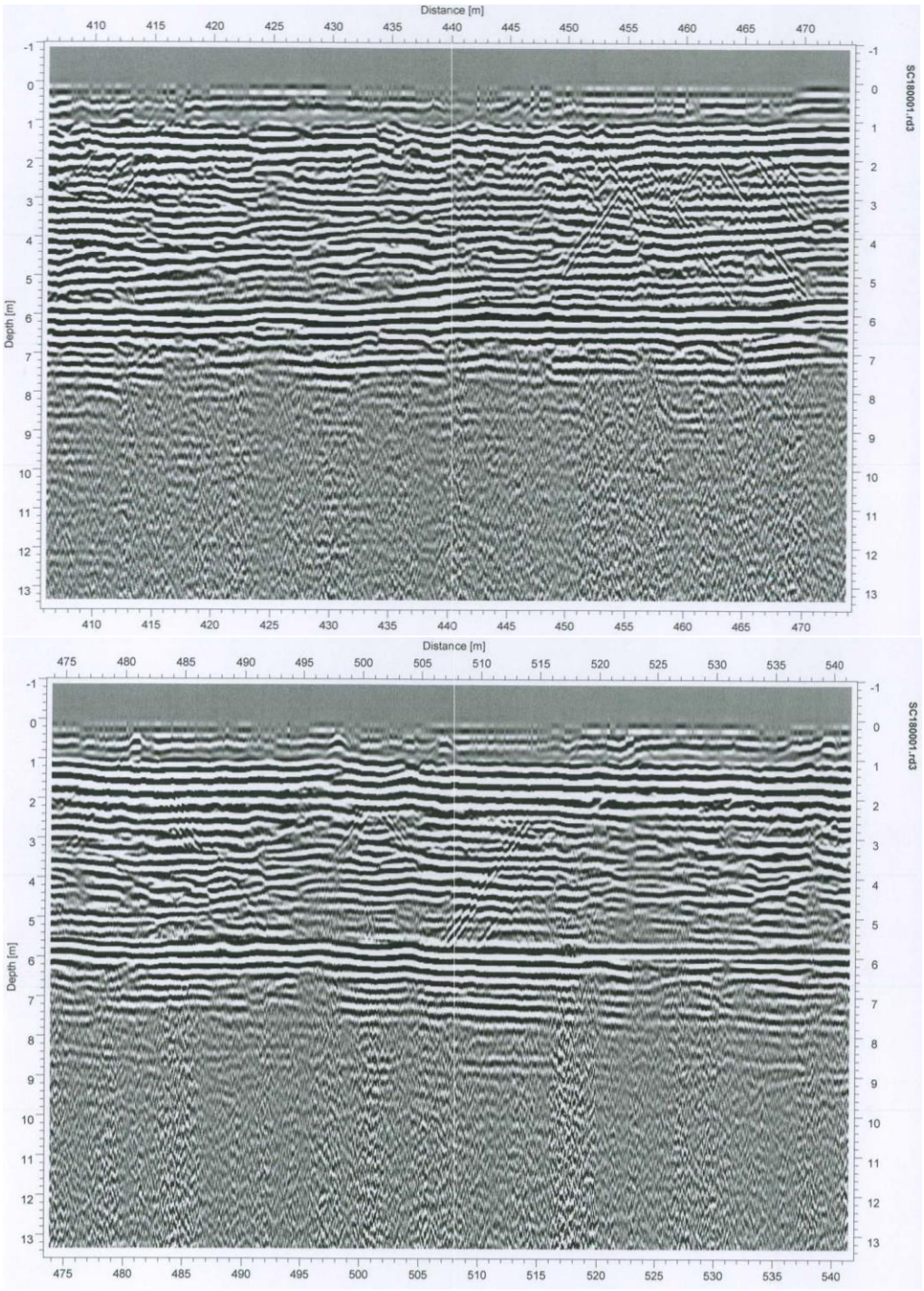
Distance [m]
410 415 420 425 430 435 440 445 450 455 460 465 470
Depth [m]
-1 0 1 2 3 4 5 6 7 8 9 10 11 12 13
SC180001.rd3
Distance [m]
475 480 485 490 495 500 505 510 515 520 525 530 535 540
Depth [m]
-1 0 1 2 3 4 5 6 7 8 9 10 11 12 13
SC180001.rd3

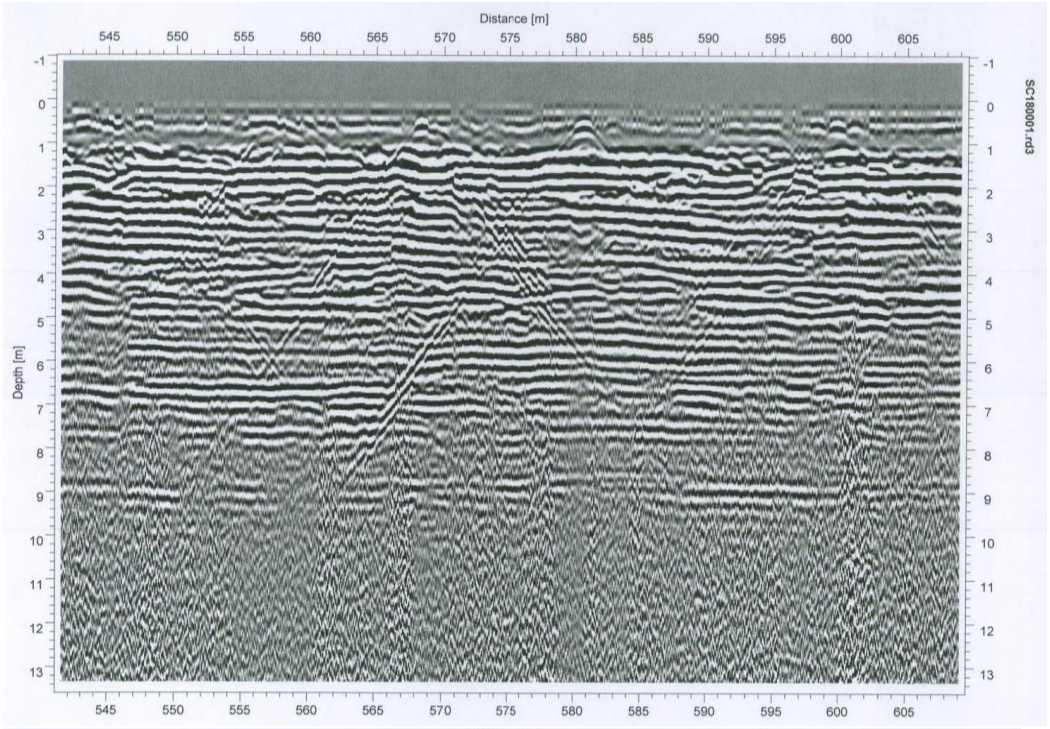
Distance [m]
545 550 555 560 565 570 575 580 585 590 595 600 605
Depth [m]
-1 0 1 2 3 4 5 6 7 8 9 10 11 12 13
SC180001.rd3

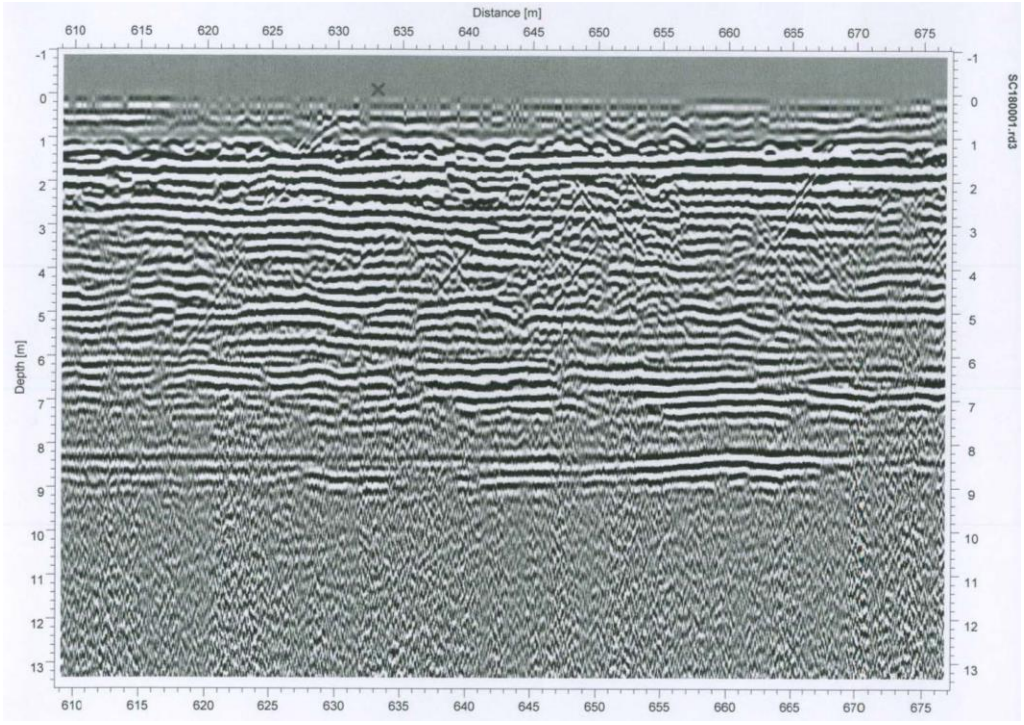
Distance [m]
610 615 620 625 630 635 640 645 650 655 660 665 670 675
Depth [m]
-1 0 1 2 3 4 5 6 7 8 9 10 11 12 13
SC180001.rd3

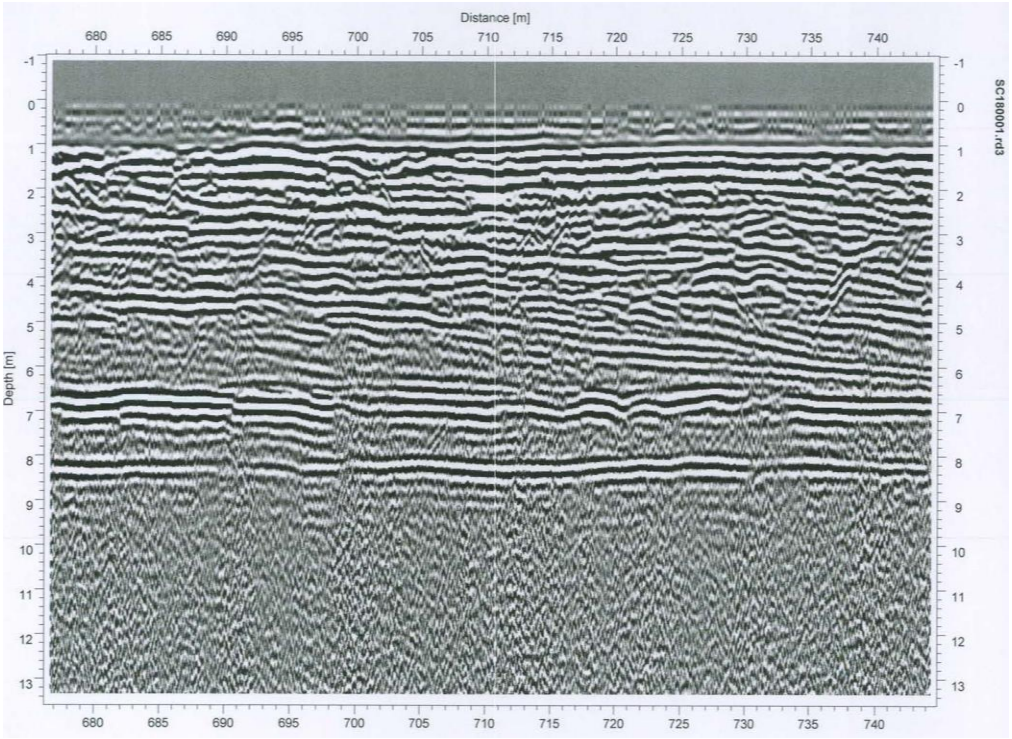
Distance [m]
680 685 690 695 700 705 710 715 720 725 730 735 740
Depth [m]
-1 0 1 2 3 4 5 6 7 8 9 10 11 12 13
SC180001.rd3

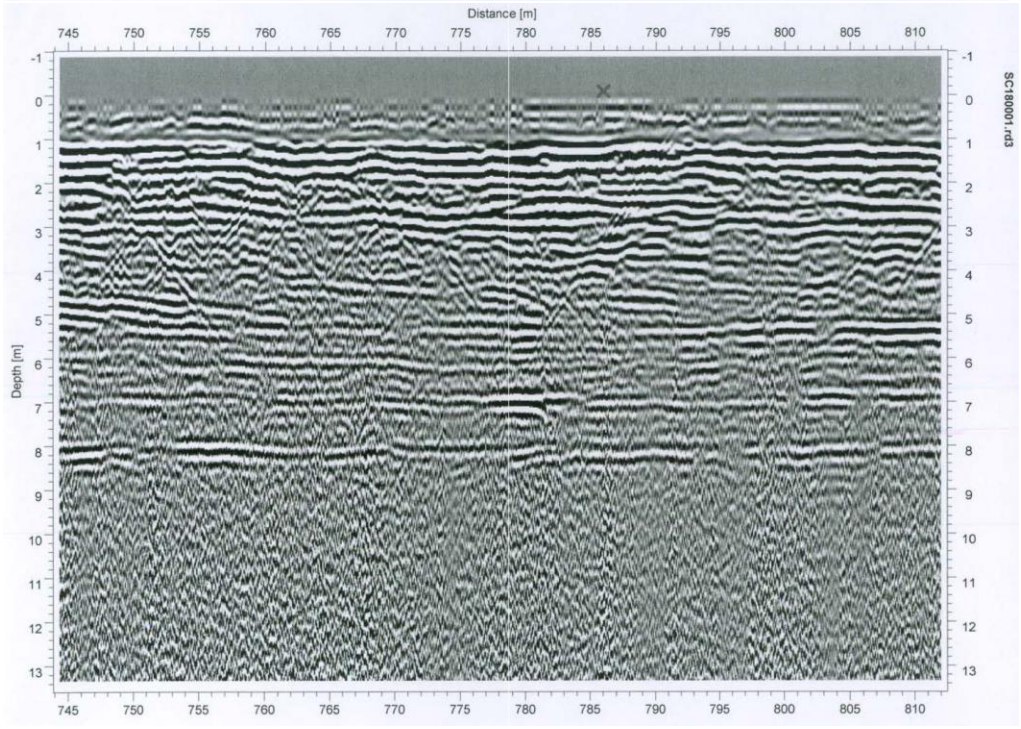
Distance [m]
745 750 755 760 765 770 775 780 785 790 795 800 805 810
Depth [m]
-1 0 1 2 3 4 5 6 7 8 9 10 11 12 13
SC180001.rd3

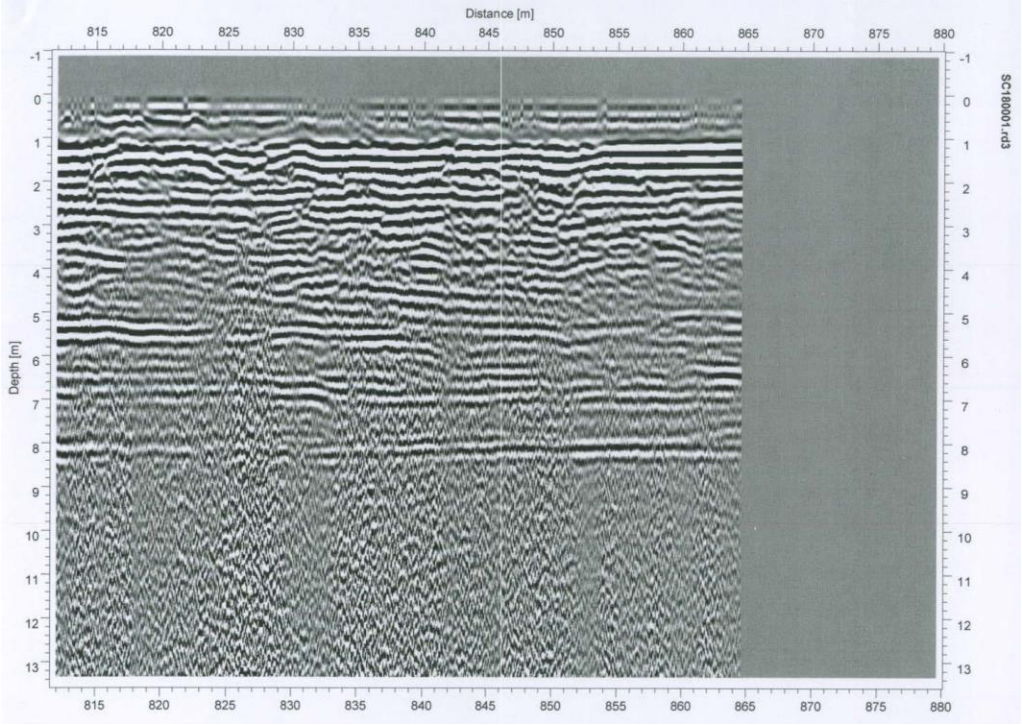

Profile 5 was run with the 100 MHz going north from Junction 24. This profile exhibits multiple sag structures and several highly attenuated layers. Excerpts of this profile are used in the results section.